Supplement of Atmos. Chem. Phys., 26, 8765–8781, 2026
https://doi.org/10.5194/acp-26-8765-2026-supplement

Atmospheric Chemistry and Physics
Open Access
EGU

Supplement of

A robust aerosol impact on clouds along the subtropical to tropical transition

Netta Yeheskel et al.

Correspondence to: Guy Dagan (guy.dagan@mail.huji.ac.il)

S1 Additional Figures

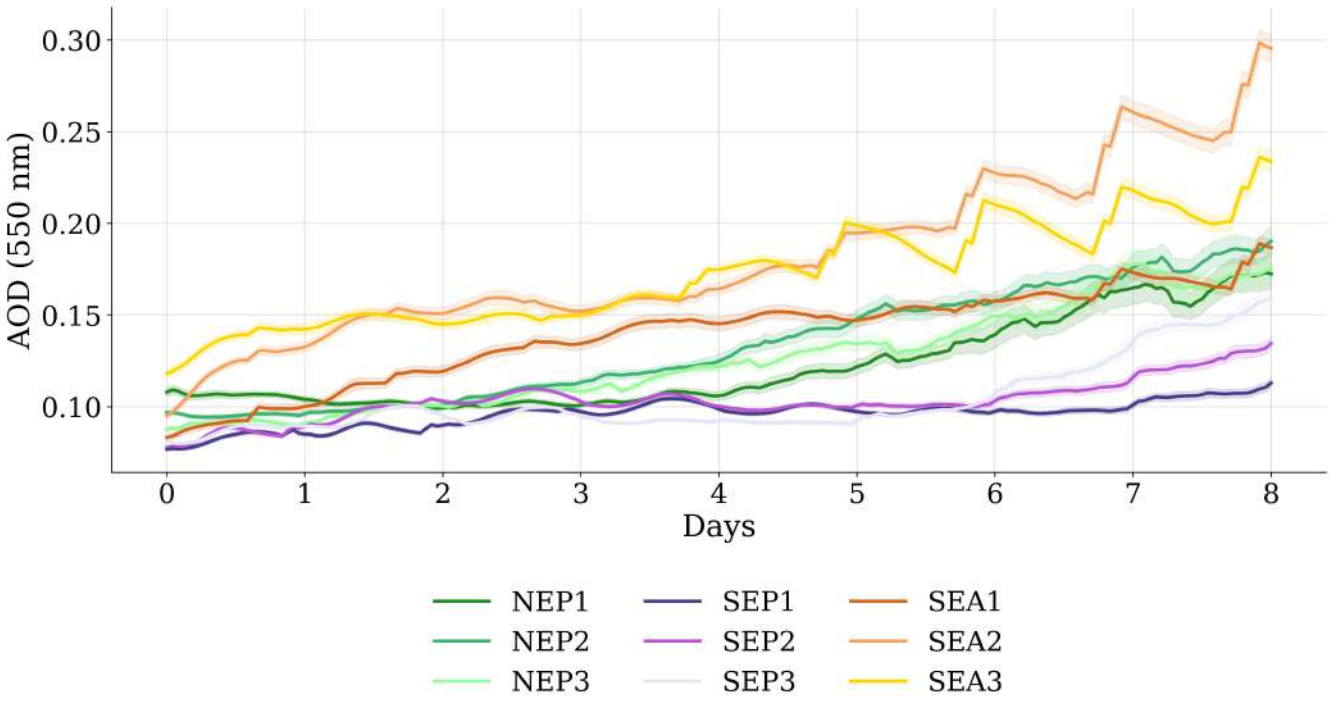

Figure S1. Mean aerosol optical depth (AOD at 550 nm) shown for all nine initial locations (NEP1-3, SEP1-3, SEA1-3). Solid lines indicate trajectory-mean AOD at each time step, and shaded areas represent the two-sided 95% confidence interval of the mean for each location, computed as mean $\pm$ 1.96 $\times$ SEM (standard error of the mean) across trajectories at each hour.

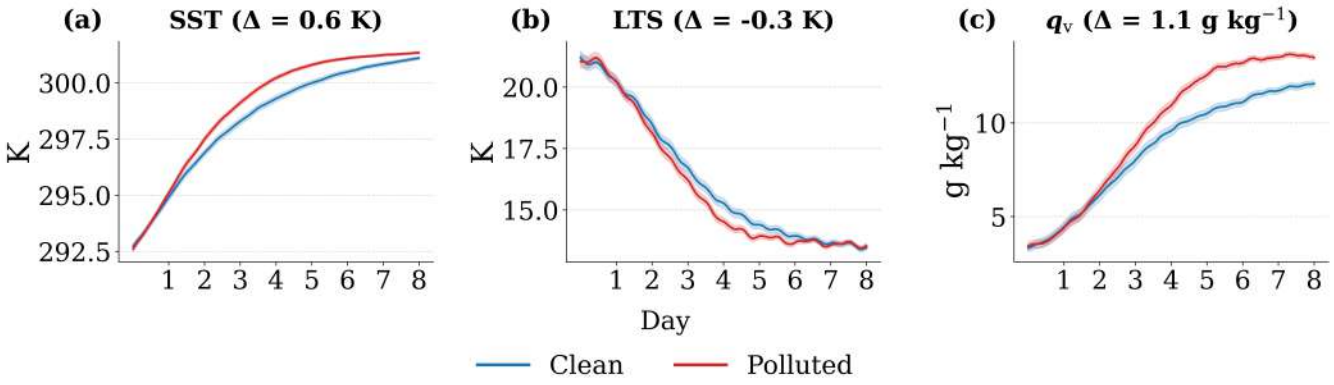

Figure S2. Hourly mean evolution of environmental variables along Lagrangian trajectories for the NEP2 initial location (28.0°N, 121.0°W), separated into clean (blue) and polluted (red) groups. Shown are: (a) sea surface temperature (SST), (b) lower-tropospheric stability (LTS), and (c) specific humidity at 850 hPa (q_v 850 hPa). Solid lines represent group means, shaded regions and error bars represent two-sided 95% confidence intervals for the mean, computed as mean $\pm$ 1.96 $\times$ SEM (standard error of the mean) across trajectories at each hour. The time-mean differences between the polluted and clean trajectories are shown in parentheses above each panel.

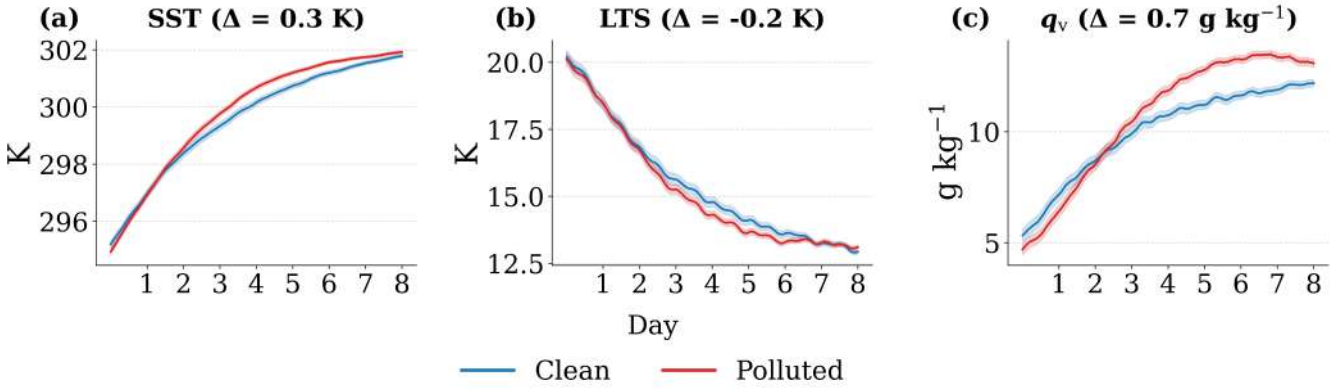

Figure S3. Hourly mean evolution of environmental variables along Lagrangian trajectories for the NEP3 initial location (24.0°N, 127.0°W), separated into clean (blue) and polluted (red) groups. Shown are: (a) sea surface temperature (SST), (b) lower-tropospheric stability (LTS), and (c) specific humidity at 850 hPa (q_v 850 hPa). Solid lines represent group means, shaded regions and error bars represent two-sided 95% confidence intervals for the mean, computed as mean $\pm$ 1.96 $\times$ SEM (standard error of the mean) across trajectories at each hour. The time-mean differences between the polluted and clean trajectories are shown in parentheses above each panel.

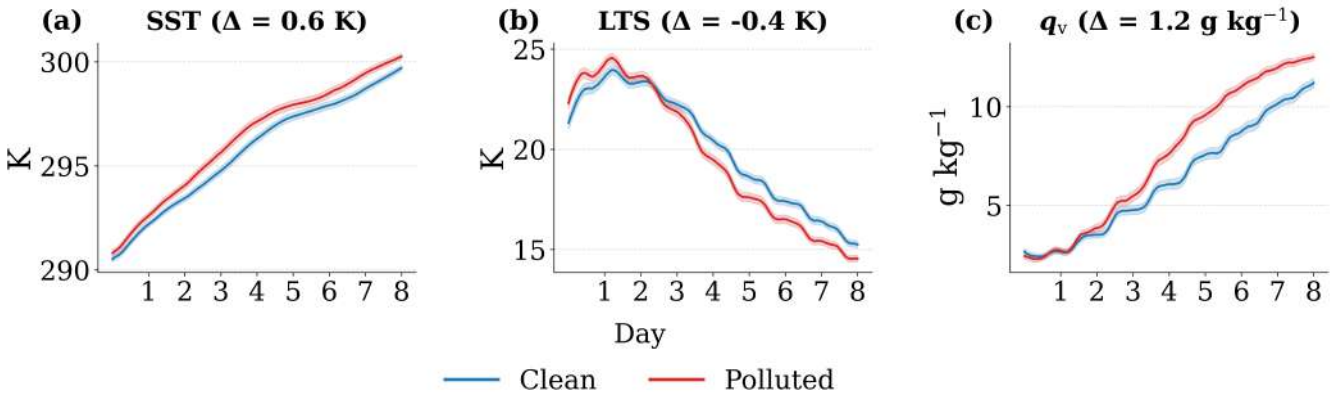

Figure S4. Hourly mean evolution of environmental variables along Lagrangian trajectories for the SEP1 initial location (30.0°S, 75.0°W), separated into clean (blue) and polluted (red) groups. Shown are: (a) sea surface temperature (SST), (b) lower-tropospheric stability (LTS), and (c) specific humidity at 850 hPa (q_v 850 hPa). Solid lines represent group means, shaded regions and error bars represent two-sided 95% confidence intervals for the mean, computed as mean $\pm$ 1.96 $\times$ SEM (standard error of the mean) across trajectories at each hour. The time-mean differences between the polluted and clean trajectories are shown in parentheses above each panel.

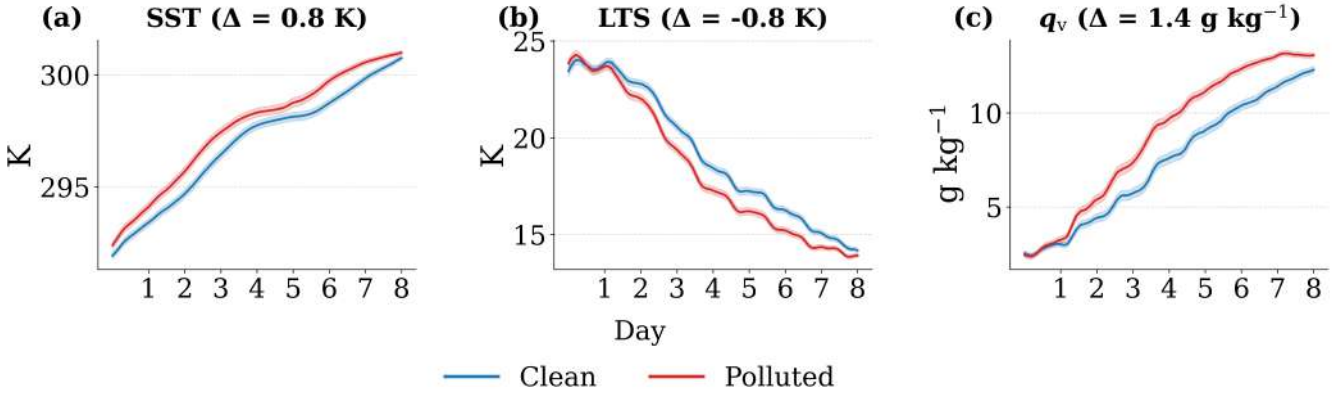

Figure S5. Hourly mean evolution of environmental variables along Lagrangian trajectories for the SEP2 initial location (25.0°S, 75.0°W), separated into clean (blue) and polluted (red) groups. Shown are: (a) sea surface temperature (SST), (b) lower-tropospheric stability (LTS), and (c) specific humidity at 850 hPa (q_v 850 hPa). Solid lines represent group means, shaded regions and error bars represent two-sided 95% confidence intervals for the mean, computed as mean $\pm$ 1.96 $\times$ SEM (standard error of the mean) across trajectories at each hour. The time-mean differences between the polluted and clean trajectories are shown in parentheses above each panel.

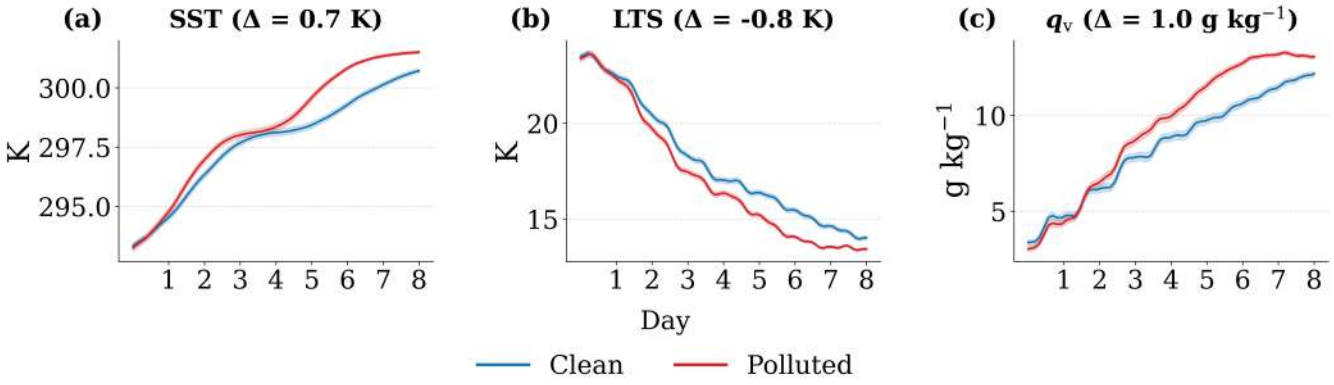

Figure S6. Hourly mean evolution of environmental variables along Lagrangian trajectories for the SEP3 initial location (20.0°S, 80.0°W), separated into clean (blue) and polluted (red) groups. Shown are: (a) sea surface temperature (SST), (b) lower-tropospheric stability (LTS), and (c) specific humidity at 850 hPa (q_v 850 hPa). Solid lines represent group means, shaded regions and error bars represent two-sided 95% confidence intervals for the mean, computed as mean $\pm$ 1.96 $\times$ SEM (standard error of the mean) across trajectories at each hour. The time-mean differences between the polluted and clean trajectories are shown in parentheses above each panel.

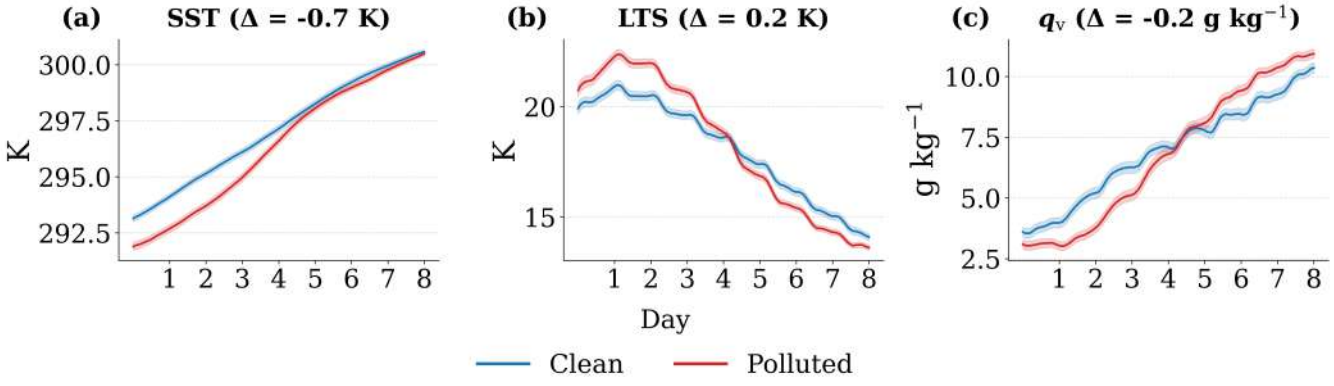

Figure S7. Hourly mean evolution of environmental variables along Lagrangian trajectories for the SEA1 initial location (30.0°S, 10.0°E), separated into clean (blue) and polluted (red) groups. Shown are: (a) sea surface temperature (SST), (b) lower-tropospheric stability (LTS), and (c) specific humidity at 850 hPa (q_v 850 hPa). Solid lines represent group means, shaded regions and error bars represent two-sided 95% confidence intervals for the mean, computed as mean $\pm$ 1.96 $\times$ SEM (standard error of the mean) across trajectories at each hour. The time-mean differences between the polluted and clean trajectories are shown in parentheses above each panel.

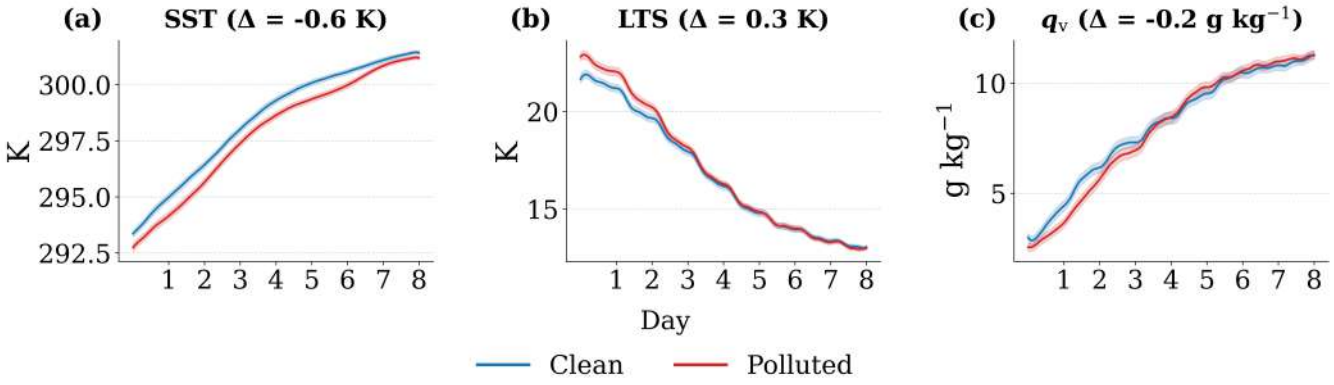

Figure S8. Hourly mean evolution of environmental variables along Lagrangian trajectories for the SEA2 initial location (25.0°S, 10.0°E), separated into clean (blue) and polluted (red) groups. Shown are: (a) sea surface temperature (SST), (b) lower-tropospheric stability (LTS), and (c) specific humidity at 850 hPa (q_v 850 hPa). Solid lines represent group means, shaded regions and error bars represent two-sided 95% confidence intervals for the mean, computed as mean $\pm$ 1.96 $\times$ SEM (standard error of the mean) across trajectories at each hour. The time-mean differences between the polluted and clean trajectories are shown in parentheses above each panel.

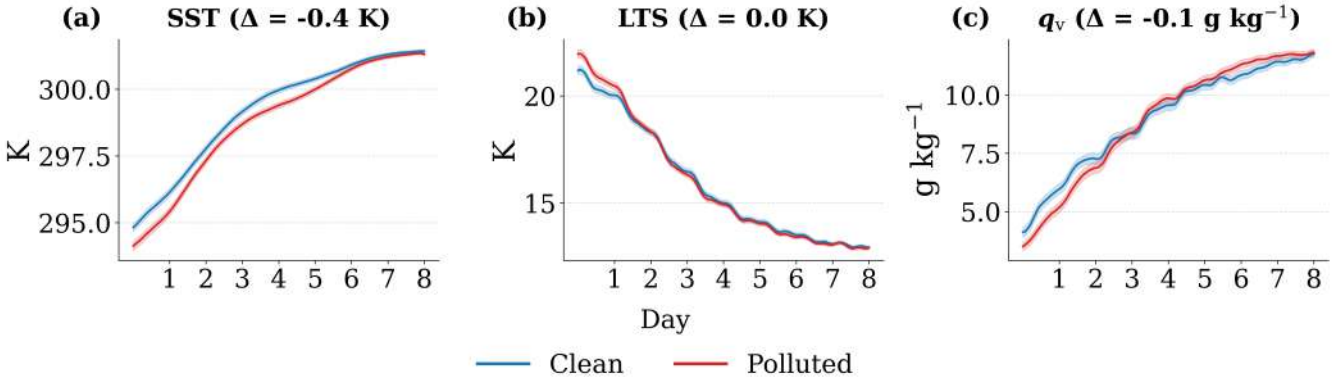

Figure S9. Hourly mean evolution of environmental variables along Lagrangian trajectories for the SEA3 initial location (20.0°S, 5.0°E), separated into clean (blue) and polluted (red) groups. Shown are: (a) sea surface temperature (SST), (b) lower-tropospheric stability (LTS), and (c) specific humidity at 850 hPa (q_v 850 hPa). Solid lines represent group means, shaded regions and error bars represent two-sided 95% confidence intervals for the mean, computed as mean $\pm$ 1.96 $\times$ SEM (standard error of the mean) across trajectories at each hour. The time-mean differences between the polluted and clean trajectories are shown in parentheses above each panel.

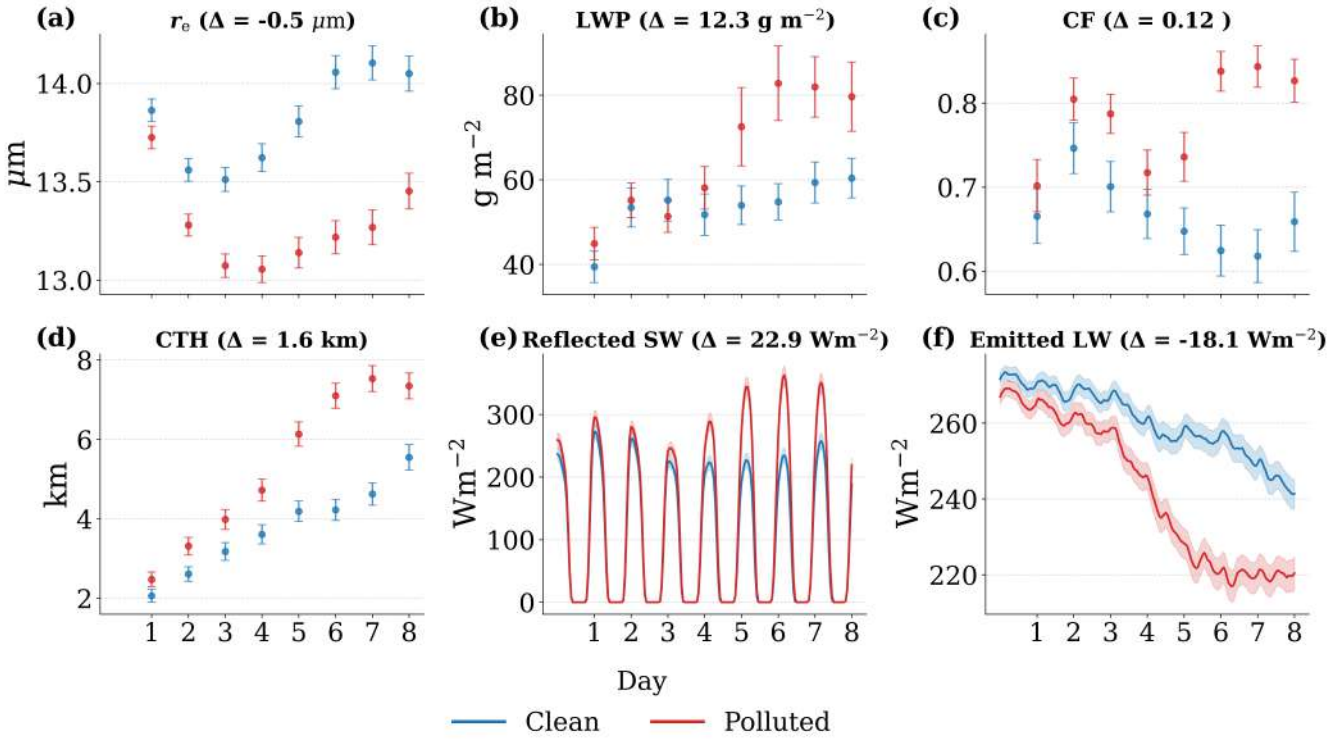

Figure S10. Mean evolution of cloud and radiation properties along Lagrangian trajectories for the NEP2 initial location (28.0°N, 121.0°W), separated into clean (blue) and polluted (red) groups. Panels (a–d) show daily means; panels (e–f) show hourly values. Shown are: (a) cloud droplet effective radius (r_e), (b) liquid water path (LWP), (c) total cloud fraction (CF), (d) cloud top height (CTH), (e) reflected shortwave radiation at Top-Of-Atmosphere (Reflected SW; TOA), and (f) emitted longwave radiation at TOA (Emitted LW). Solid lines represent group means, shaded regions and error bars represent two-sided 95% confidence intervals for the mean, computed as mean$\pm 1.96\times$ SEM (standard error of the mean) across trajectories at each hour. The time-mean differences between the polluted and clean trajectories are shown in parentheses above each panel.

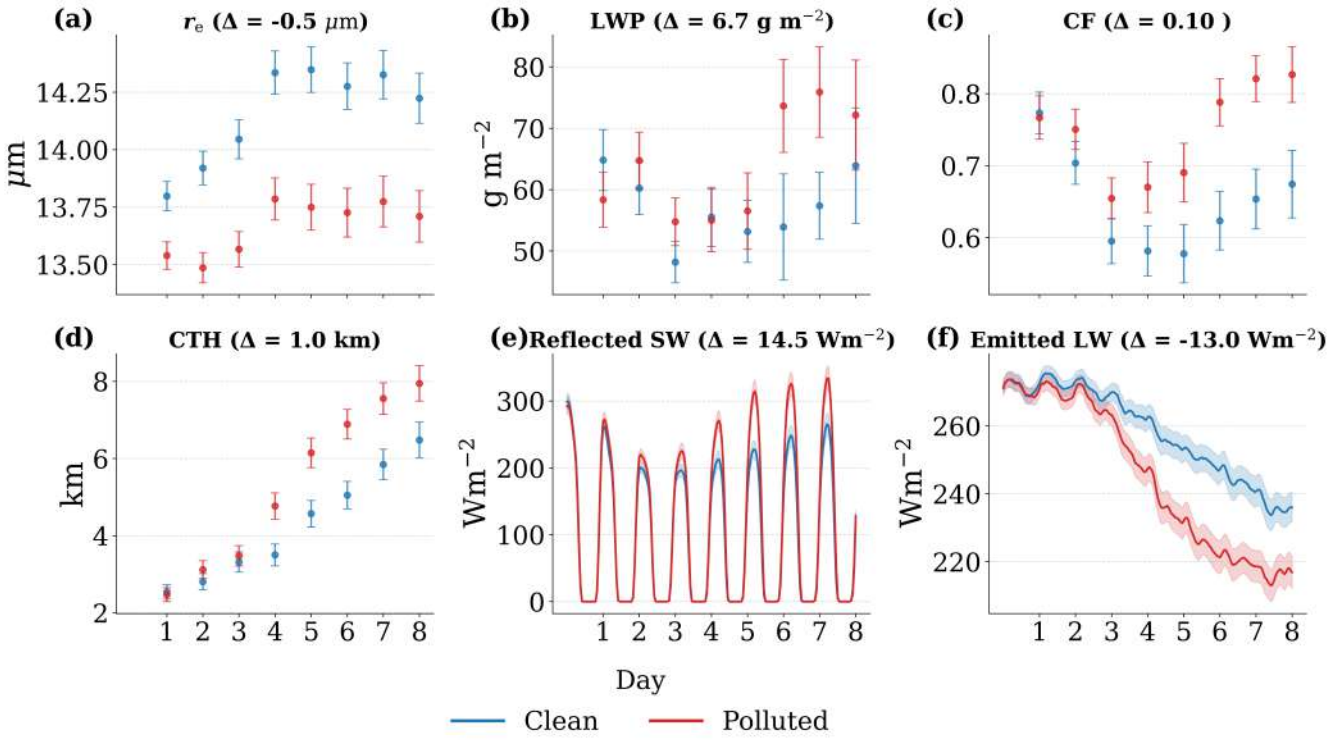

Figure S11. Mean evolution of cloud and radiation properties along Lagrangian trajectories for the NEP3 initial location (24.0°N, 127.0°W), separated into clean (blue) and polluted (red) groups. Panels (a–d) show daily means; panels (e–f) show hourly values. Shown are: (a) cloud droplet effective radius (r_e), (b) liquid water path (LWP), (c) total cloud fraction (CF), (d) cloud top height (CTH), (e) reflected shortwave radiation at Top-Of-Atmosphere (Reflected SW; TOA), and (f) emitted longwave radiation at TOA (Emitted LW). Solid lines represent group means, shaded regions and error bars represent two-sided 95% confidence intervals for the mean, computed as mean$\pm 1.96\times$ SEM (standard error of the mean) across trajectories at each hour. The time-mean differences between the polluted and clean trajectories are shown in parentheses above each panel.

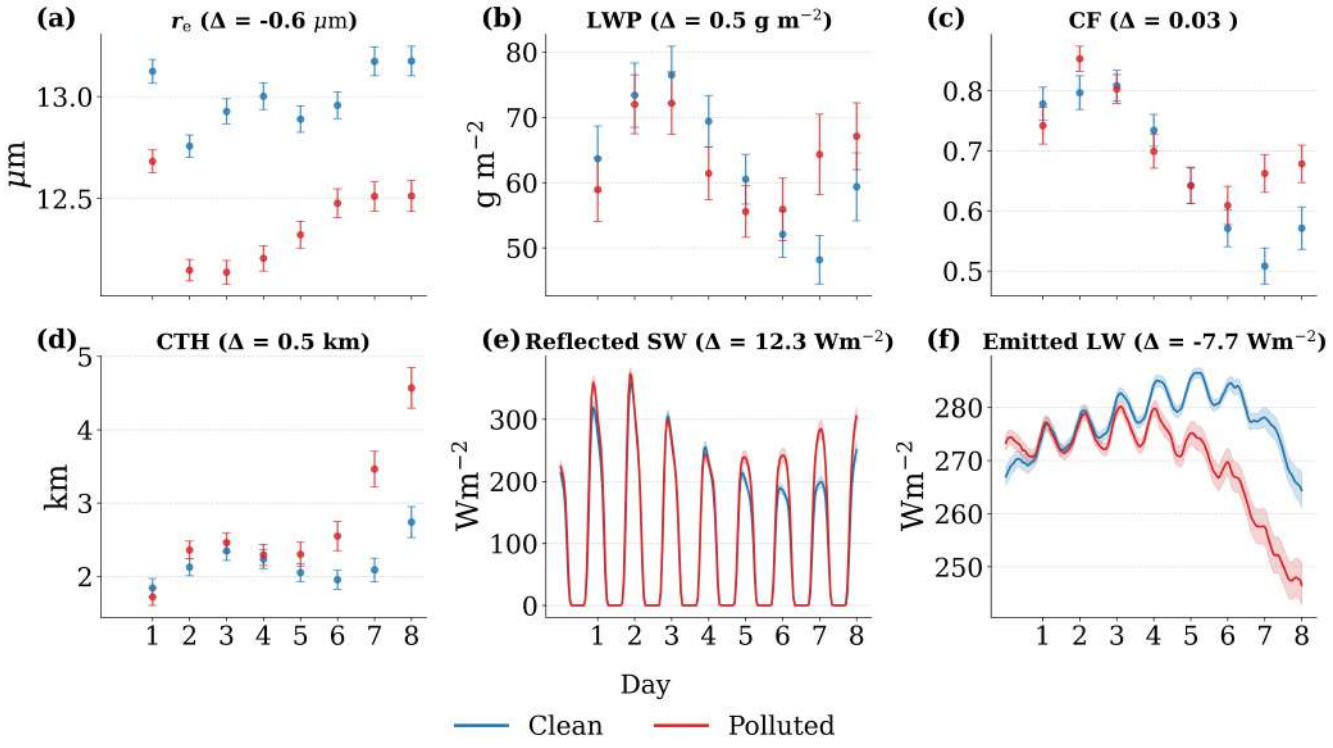

Figure S12. Mean evolution of cloud and radiation properties along Lagrangian trajectories for the SEP1 initial location (30.0°S, 75.0°W), separated into clean (blue) and polluted (red) groups. Panels (a–d) show daily means; panels (e–f) show hourly values. Shown are: (a) cloud droplet effective radius (r_e), (b) liquid water path (LWP), (c) total cloud fraction (CF), (d) cloud top height (CTH), (e) reflected shortwave radiation at Top-Of-Atmosphere (Reflected SW; TOA), and (f) emitted longwave radiation at TOA (Emitted LW). Solid lines represent group means, shaded regions and error bars represent two-sided 95% confidence intervals for the mean, computed as mean$\pm 1.96\times$ SEM (standard error of the mean) across trajectories at each hour. The time-mean differences between the polluted and clean trajectories are shown in parentheses above each panel.

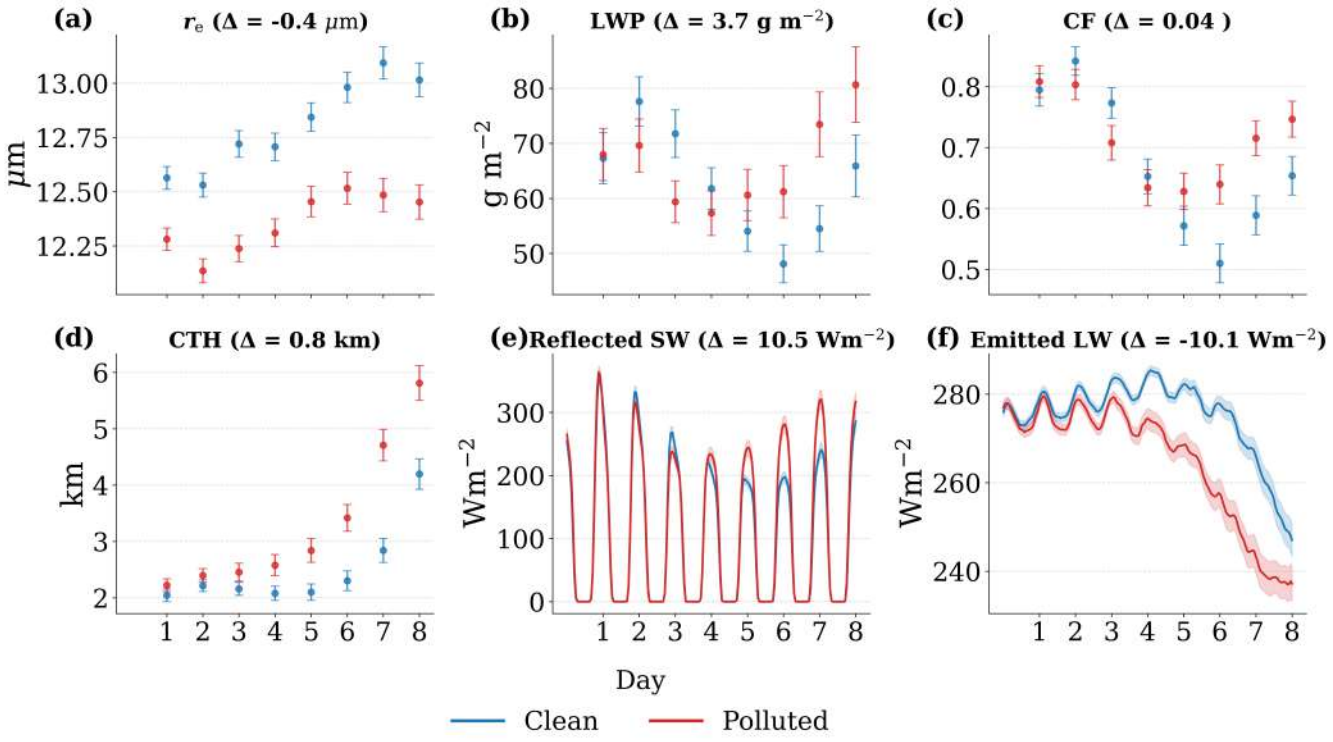

Figure S13. Mean evolution of cloud and radiation properties along Lagrangian trajectories for the SEP2 initial location (25.0°S, 75.0°W), separated into clean (blue) and polluted (red) groups. Panels (a–d) show daily means; panels (e–f) show hourly values. Shown are: (a) cloud droplet effective radius (r_e), (b) liquid water path (LWP), (c) total cloud fraction (CF), (d) cloud top height (CTH), (e) reflected shortwave radiation at Top-Of-Atmosphere (Reflected SW; TOA), and (f) emitted longwave radiation at TOA (Emitted LW). Solid lines represent group means, shaded regions and error bars represent two-sided 95% confidence intervals for the mean, computed as mean$\pm 1.96\times$ SEM (standard error of the mean) across trajectories at each hour. The time-mean differences between the polluted and clean trajectories are shown in parentheses above each panel.

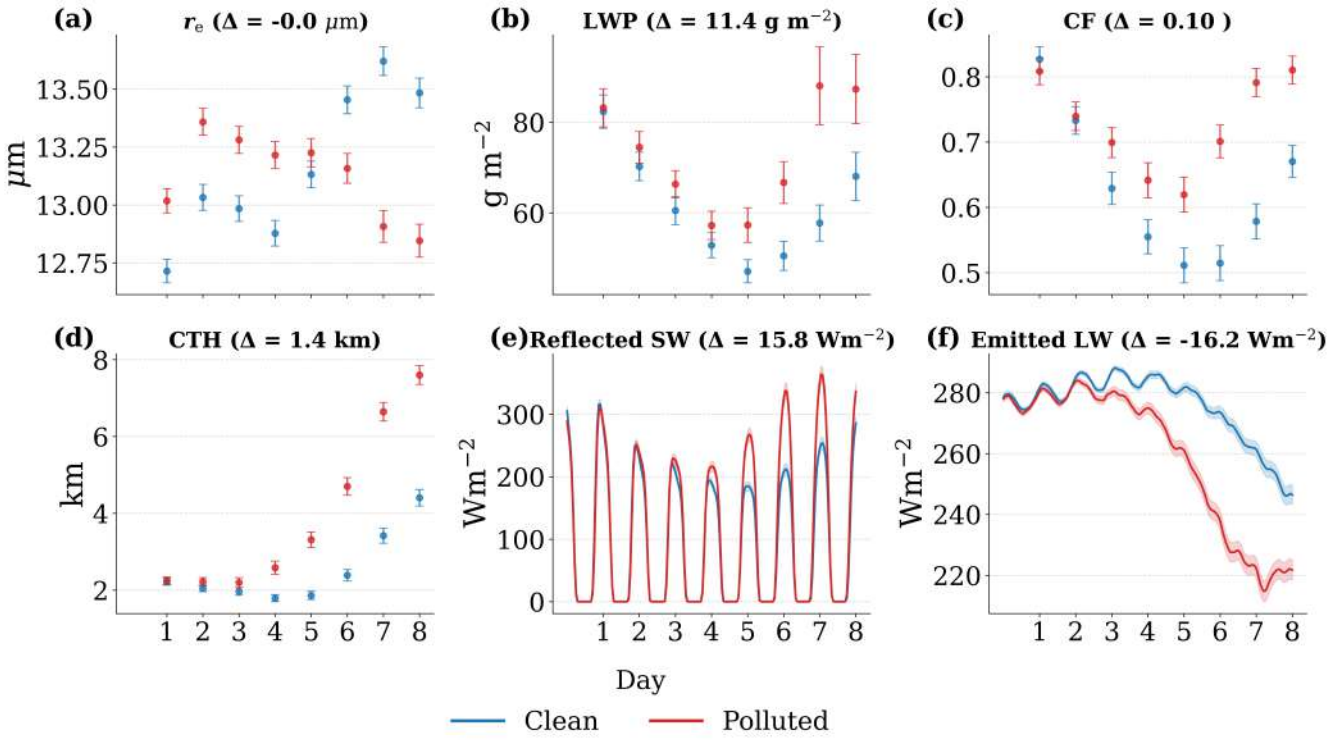

Figure S14. Mean evolution of cloud and radiation properties along Lagrangian trajectories for the SEP3 initial location (20.0°S, 80.0°W), separated into clean (blue) and polluted (red) groups. Panels (a–d) show daily means; panels (e–f) show hourly values. Shown are: (a) cloud droplet effective radius (r_e), (b) liquid water path (LWP), (c) total cloud fraction (CF), (d) cloud top height (CTH), (e) reflected shortwave radiation at Top-Of-Atmosphere (Reflected SW; TOA), and (f) emitted longwave radiation at TOA (Emitted LW). Solid lines represent group means, shaded regions and error bars represent two-sided 95% confidence intervals for the mean, computed as mean$\pm 1.96\times$ SEM (standard error of the mean) across trajectories at each hour. The time-mean differences between the polluted and clean trajectories are shown in parentheses above each panel.

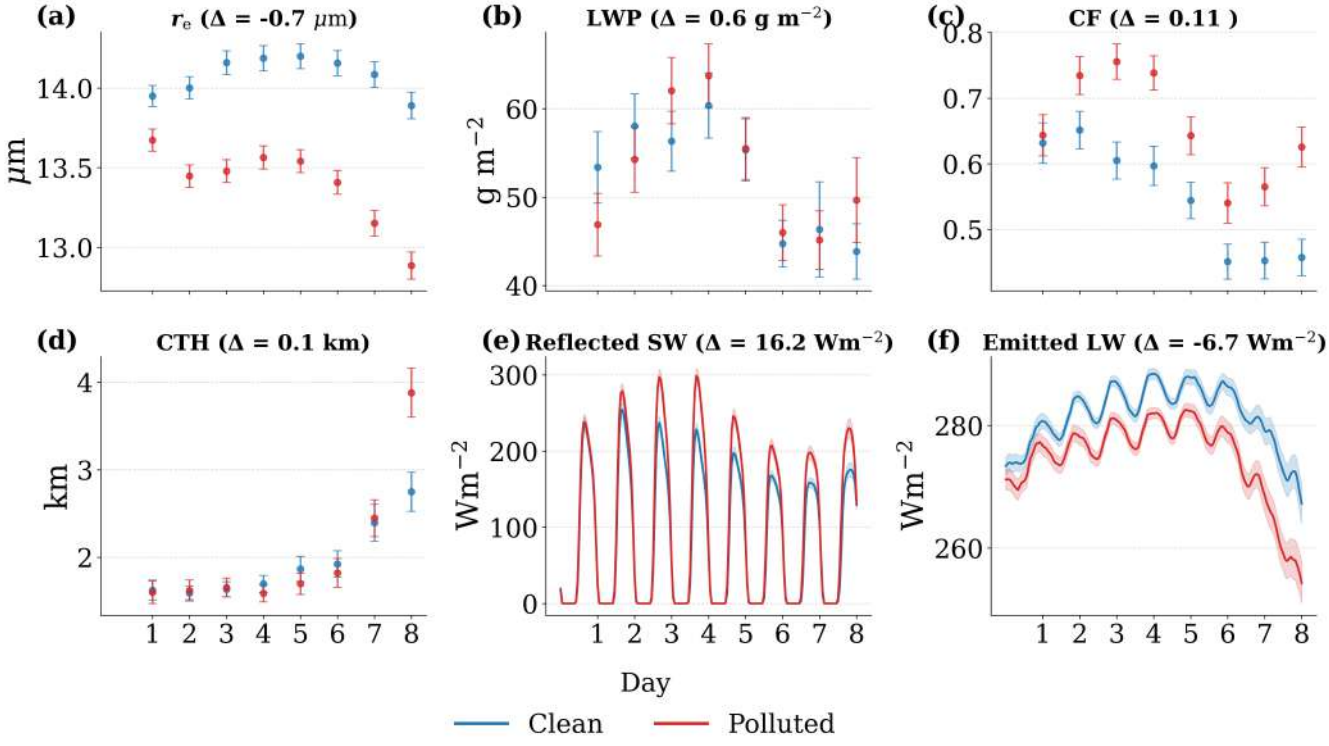

Figure S15. Mean evolution of cloud and radiation properties along Lagrangian trajectories for the SEA1 initial location (30.0°S, 10.0°E), separated into clean (blue) and polluted (red) groups. Panels (a–d) show daily means; panels (e–f) show hourly values. Shown are: (a) cloud droplet effective radius (r_e), (b) liquid water path (LWP), (c) total cloud fraction (CF), (d) cloud top height (CTH), (e) reflected shortwave radiation at Top-Of-Atmosphere (Reflected SW; TOA), and (f) emitted longwave radiation at TOA (Emitted LW). Solid lines represent group means, shaded regions and error bars represent two-sided 95% confidence intervals for the mean, computed as mean$\pm 1.96\times$ SEM (standard error of the mean) across trajectories at each hour. The time-mean differences between the polluted and clean trajectories are shown in parentheses above each panel.

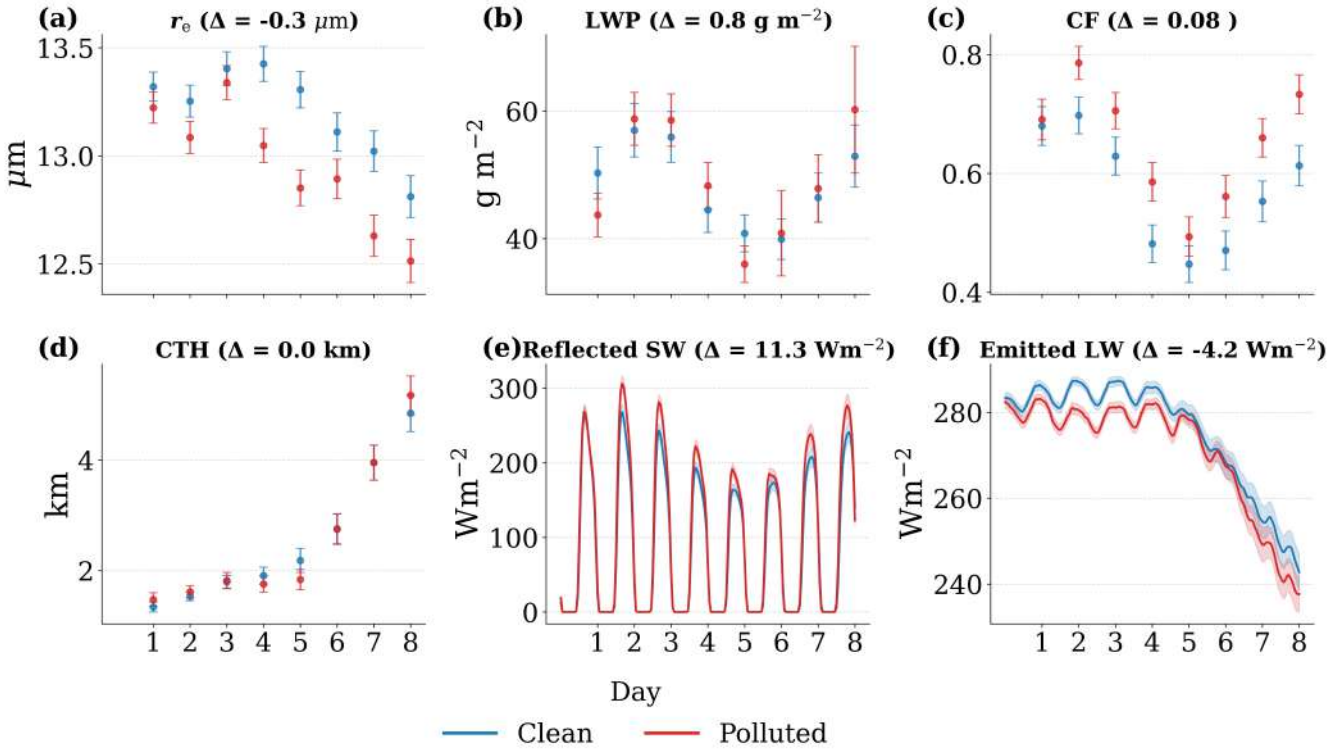

Figure S16. Mean evolution of cloud and radiation properties along Lagrangian trajectories for the SEA2 initial location (25.0°S, 10.0°E), separated into clean (blue) and polluted (red) groups. Panels (a–d) show daily means; panels (e–f) show hourly values. Shown are: (a) cloud droplet effective radius (r_e), (b) liquid water path (LWP), (c) total cloud fraction (CF), (d) cloud top height (CTH), (e) reflected shortwave radiation at Top-Of-Atmosphere (Reflected SW; TOA), and (f) emitted longwave radiation at TOA (Emitted LW). Solid lines represent group means, shaded regions and error bars represent two-sided 95% confidence intervals for the mean, computed as mean $\pm 1.96 \times$ SEM (standard error of the mean) across trajectories at each hour. The time-mean differences between the polluted and clean trajectories are shown in parentheses above each panel.

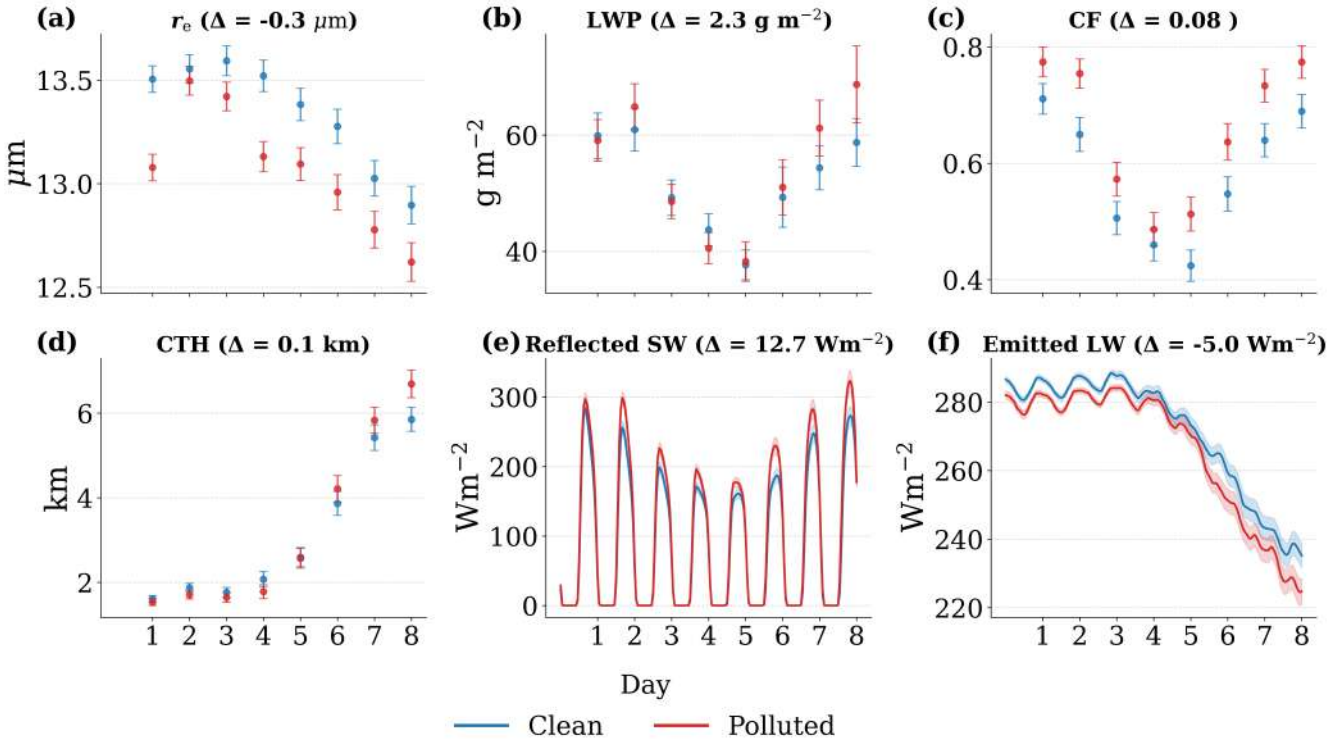

Figure S17. Mean evolution of cloud and radiation properties along Lagrangian trajectories for the SEA3 initial location (20.0°S, 5.0°E), separated into clean (blue) and polluted (red) groups. Panels (a–d) show daily means; panels (e–f) show hourly values. Shown are: (a) cloud droplet effective radius (r_e), (b) liquid water path (LWP), (c) total cloud fraction (CF), (d) cloud top height (CTH), (e) reflected shortwave radiation at Top-Of-Atmosphere (Reflected SW; TOA), and (f) emitted longwave radiation at TOA (Emitted LW). Solid lines represent group means, shaded regions and error bars represent two-sided 95% confidence intervals for the mean, computed as mean$\pm 1.96\times$ SEM (standard error of the mean) across trajectories at each hour. The time-mean differences between the polluted and clean trajectories are shown in parentheses above each panel.

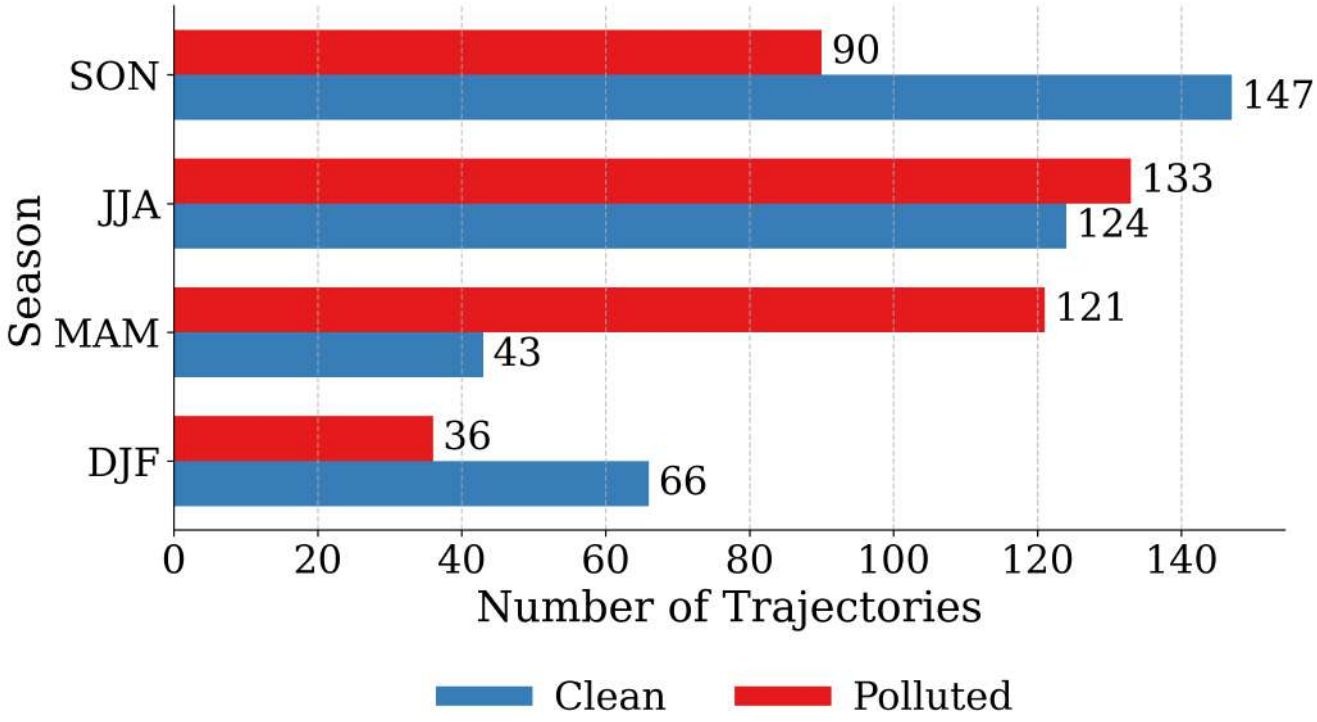

Figure S18. Seasonal distribution of trajectories by aerosol loading for the NEP1 initial location (34.0°N, 125.0°W). Horizontal bars show the number of trajectories in each season (DJF, MAM, JJA, SON) for the Low AOD (blue) and High AOD (red) groups.

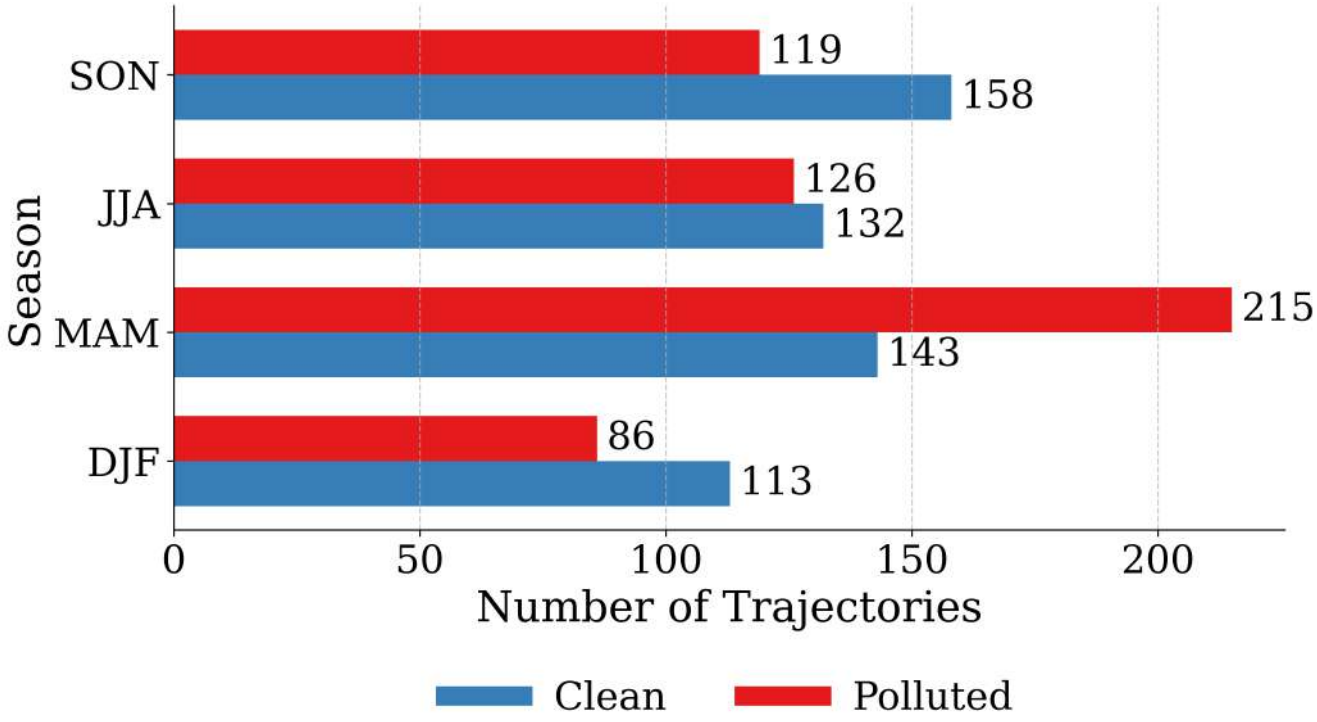

Figure S19. Seasonal distribution of trajectories by aerosol loading for the NEP2 initial location (28.0°N, 121.0°W). Horizontal bars show the number of trajectories in each season (DJF, MAM, JJA, SON) for the Low AOD (blue) and High AOD (red) groups.

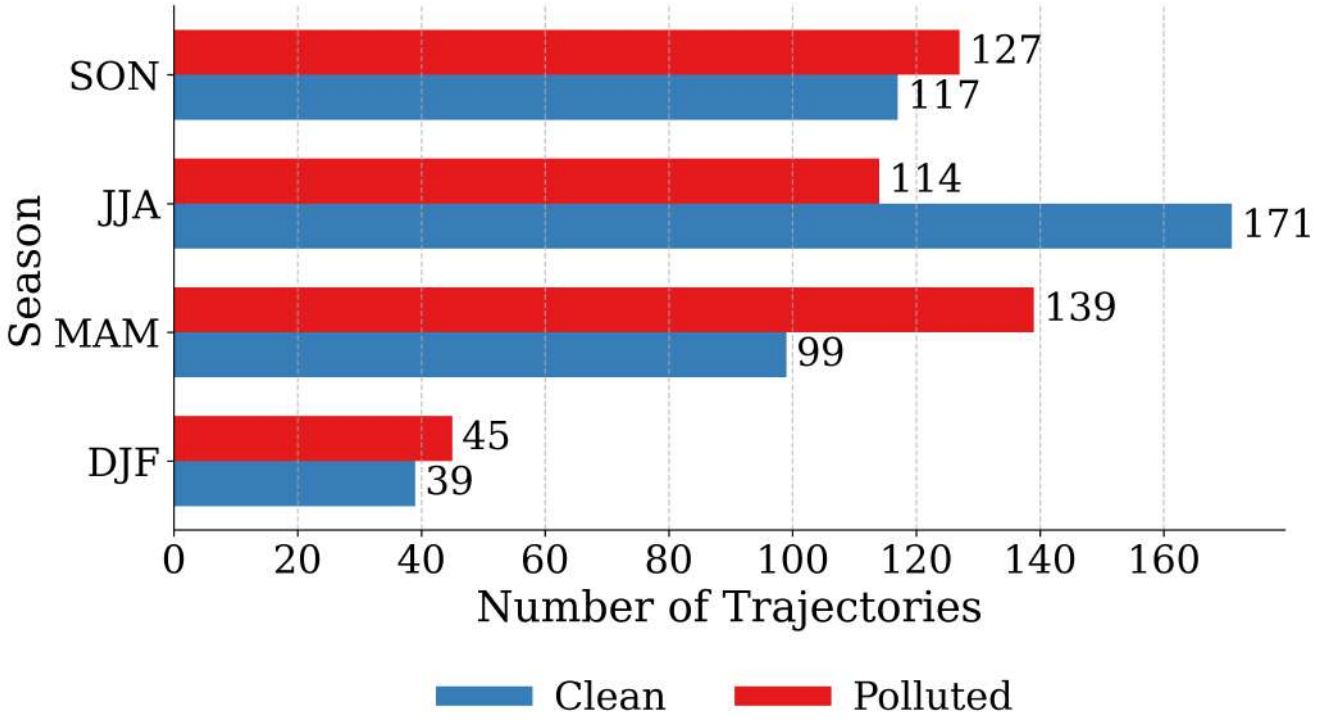

Figure S20. Seasonal distribution of trajectories by aerosol loading for the NEP3 initial location (24.0°N, 127.0°W). Horizontal bars show the number of trajectories in each season (DJF, MAM, JJA, SON) for the Low AOD (blue) and High AOD (red) groups.

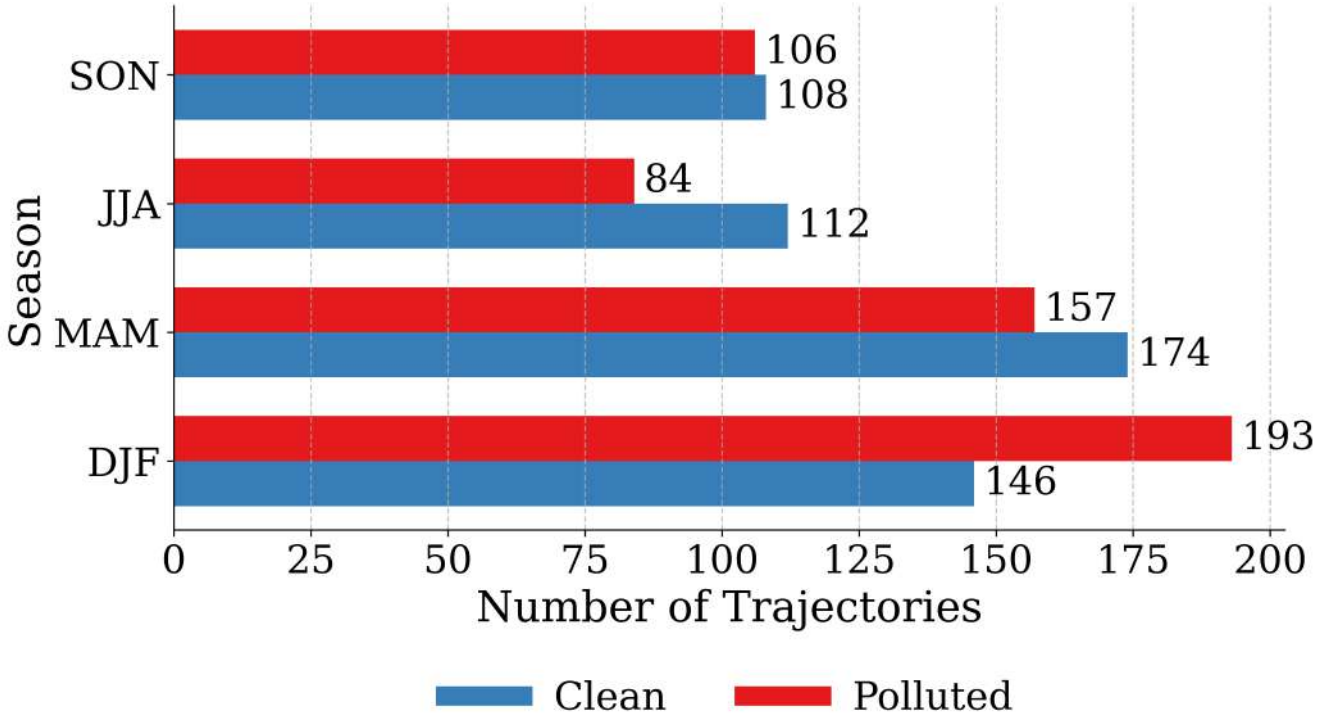

Figure S21. Seasonal distribution of trajectories by aerosol loading for the SEP1 initial location (30.0°S, 75.0°W). Horizontal bars show the number of trajectories in each season (DJF, MAM, JJA, SON) for the Low AOD (blue) and High AOD (red) groups.

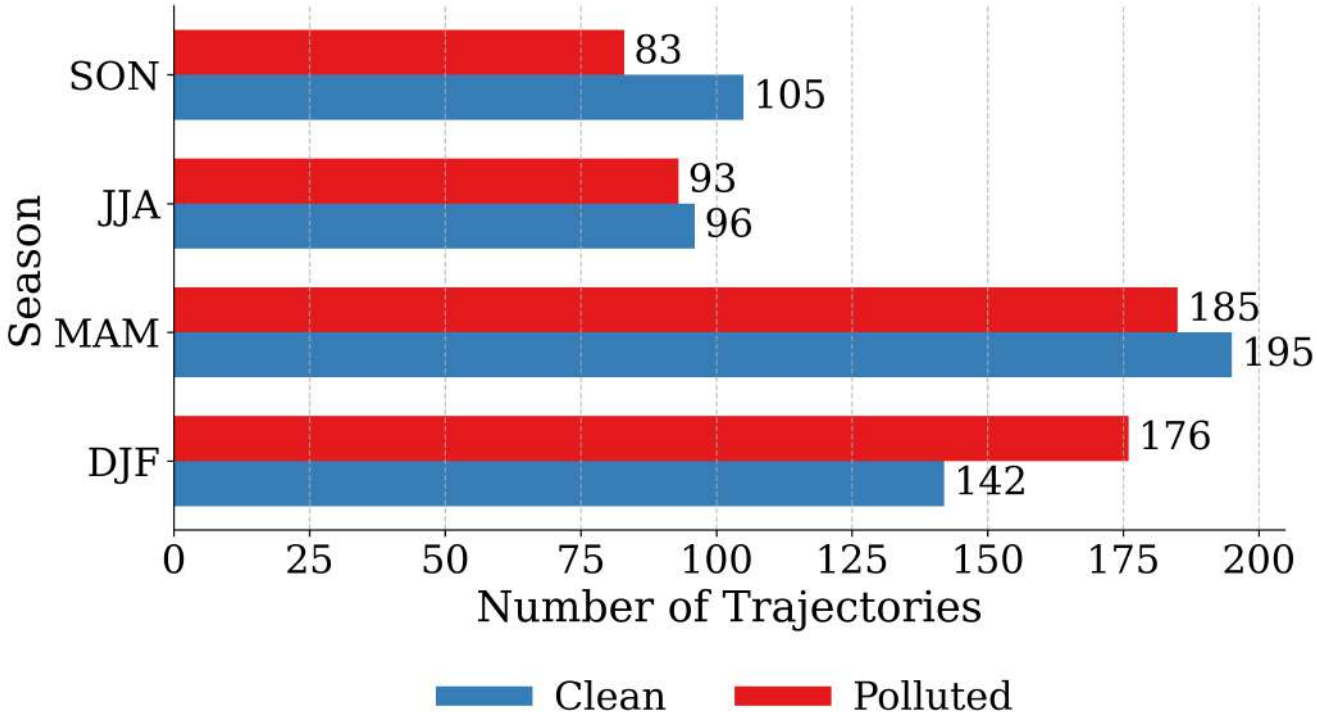

Figure S22. Seasonal distribution of trajectories by aerosol loading for the SEP2 initial location (25.0°S, 75.0°W). Horizontal bars show the number of trajectories in each season (DJF, MAM, JJA, SON) for the Low AOD (blue) and High AOD (red) groups.

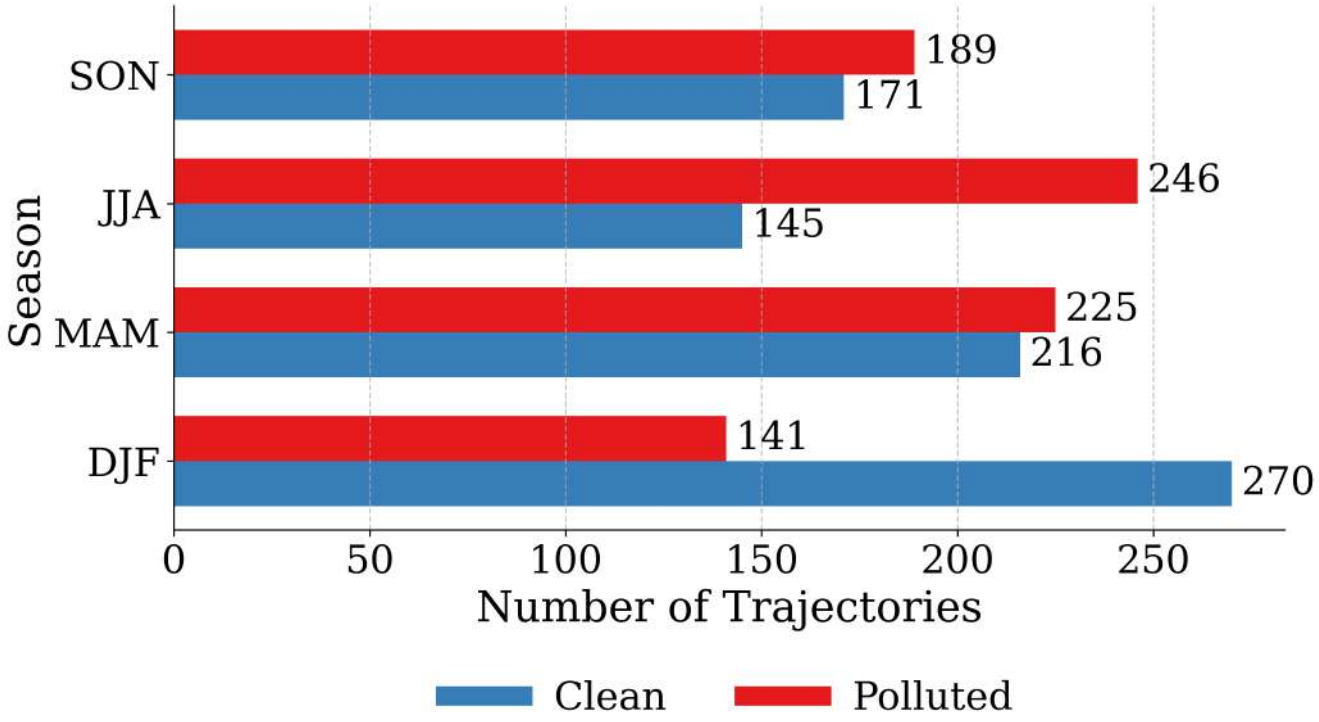

Figure S23. Seasonal distribution of trajectories by aerosol loading for the SEP3 initial location (20.0°S, 80.0°W). Horizontal bars show the number of trajectories in each season (DJF, MAM, JJA, SON) for the Low AOD (blue) and High AOD (red) groups.

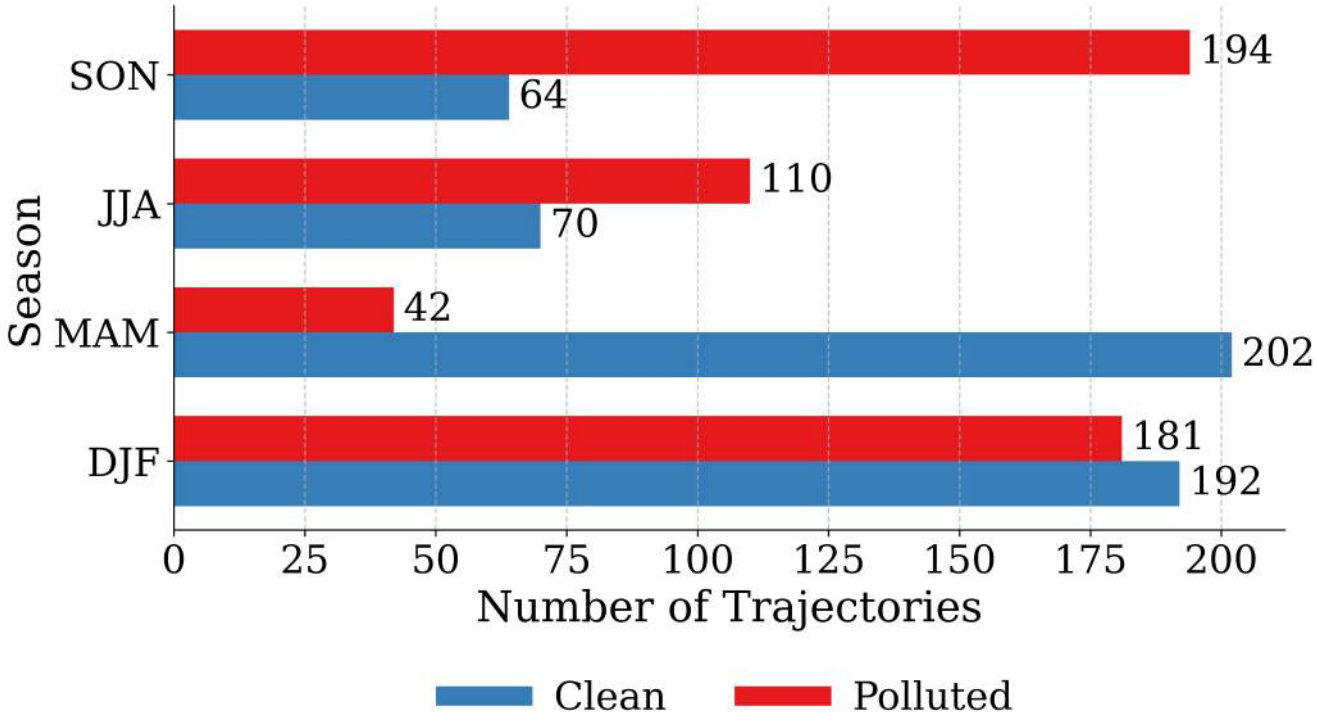

Figure S24. Seasonal distribution of trajectories by aerosol loading for the SEA1 initial location (30.0°S, 10.0°E). Horizontal bars show the number of trajectories in each season (DJF, MAM, JJA, SON) for the Low AOD (blue) and High AOD (red) groups.

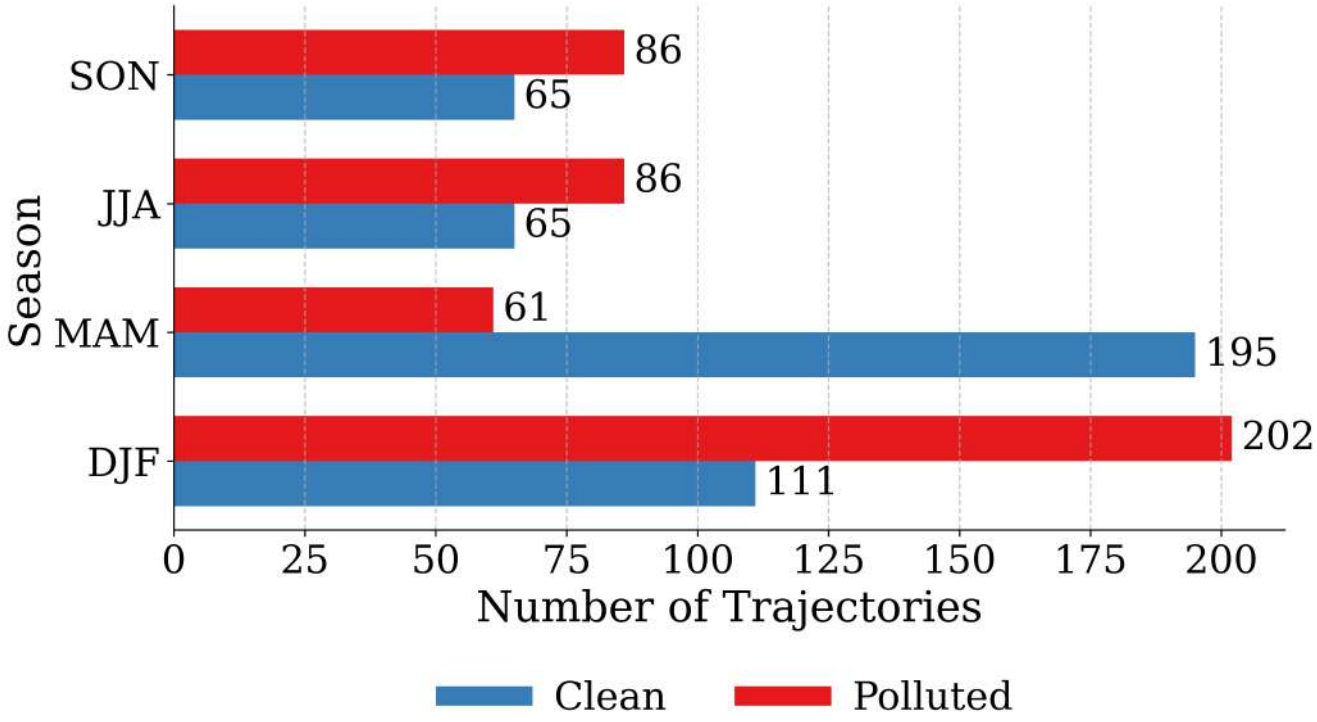

Figure S25. Seasonal distribution of trajectories by aerosol loading for the SEA2 initial location (25.0°S, 10.0°E). Horizontal bars show the number of trajectories in each season (DJF, MAM, JJA, SON) for the Low AOD (blue) and High AOD (red) groups.

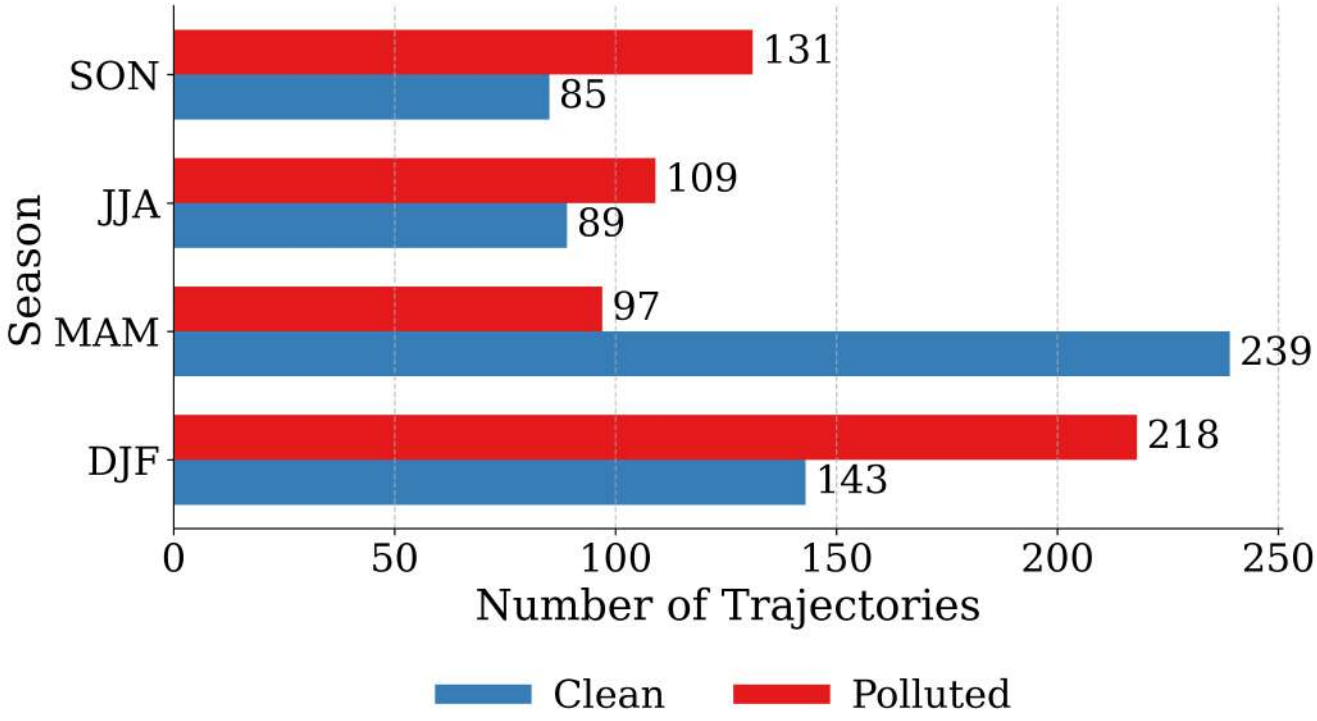

Figure S26. Seasonal distribution of trajectories by aerosol loading for the SEA3 initial location (20.0°S, 5.0°E). Horizontal bars show the number of trajectories in each season (DJF, MAM, JJA, SON) for the Low AOD (blue) and High AOD (red) groups.

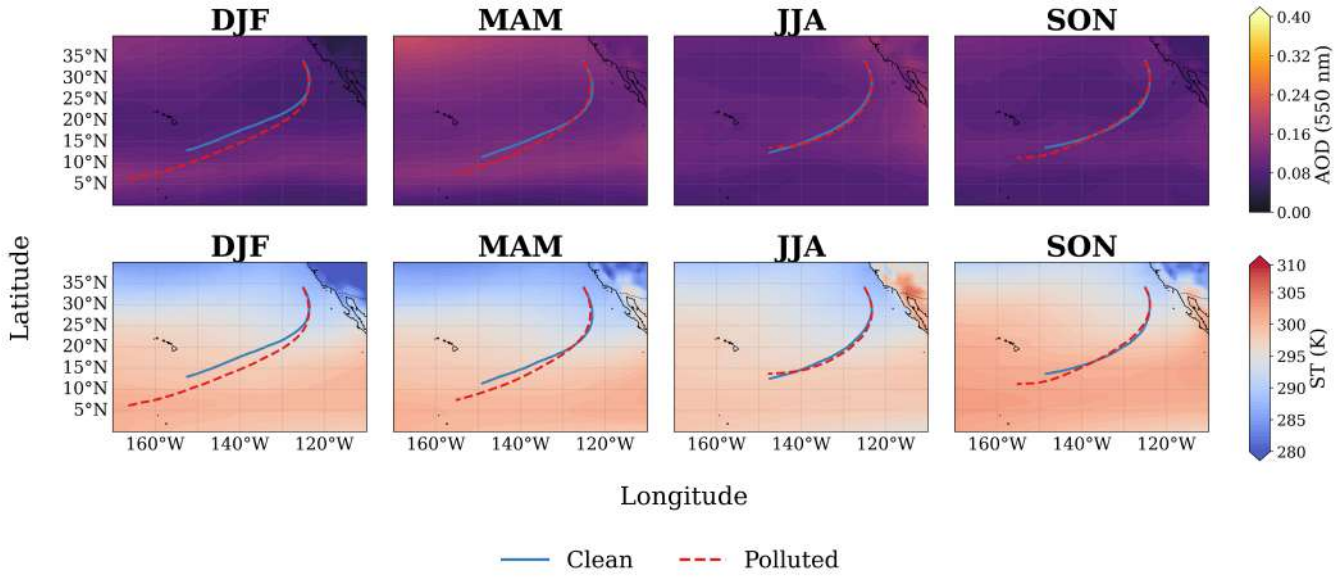

Figure S27. Seasonal mean AOD and sea surface (ST) environments for the NEP1 initial location (34.0°N, 125.0°W) trajectories, separated into clean (blue) and polluted (red, dashed) groups. The top row shows the seasonal mean AOD at 550 nm, and the bottom row shows the corresponding seasonal mean SST for each season (DJF, MAM, JJA, SON). Data from MERRA-2 reanalysis data (M2TMNXAER (DOI: (10.5067/FH9A0MLJPC7N) and M2TMNXSLV (DOI: 10.5067/AP1B0BA5PD2K) products; Global Modeling and Assimilation Office, NASA GES DISC).

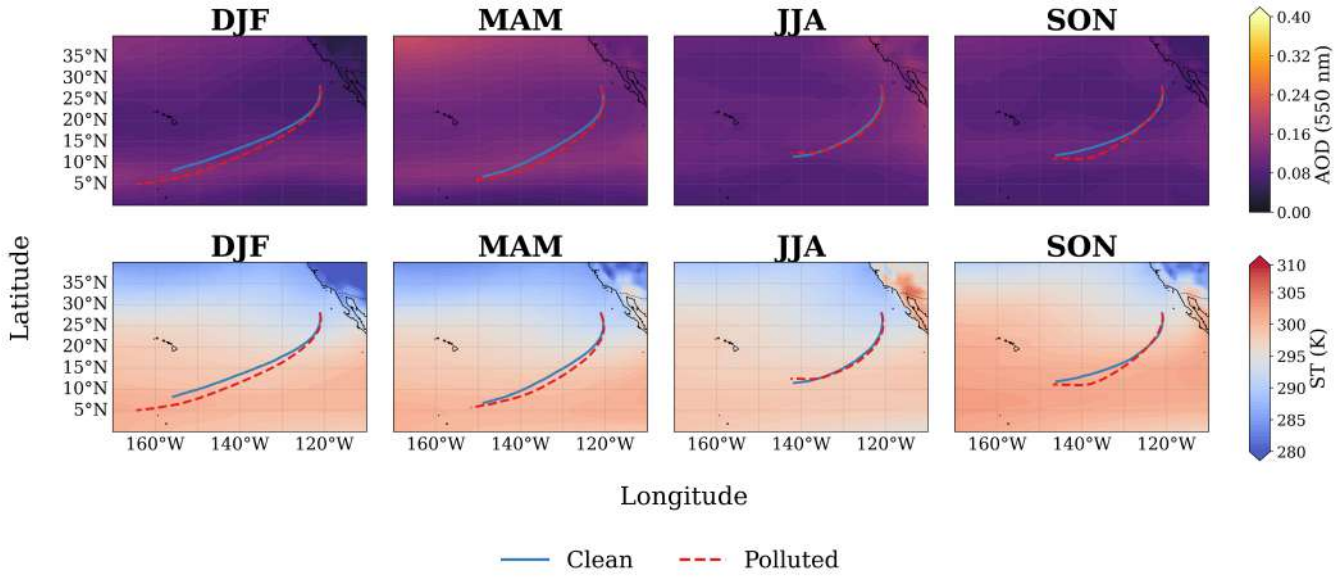

Figure S28. Seasonal mean AOD and sea surface (ST) environments for the NEP2 initial location (28.0°N, 121.0°W) trajectories, separated into clean (blue) and polluted (red, dashed) groups. The top row shows the seasonal mean AOD at 550 nm, and the bottom row shows the corresponding seasonal mean SST for each season (DJF, MAM, JJA, SON). Data from MERRA-2 reanalysis data (M2TMNXAER (DOI: (10.5067/FH9A0MLJPC7N) and M2TMNXSLV (DOI: 10.5067/AP1B0BA5PD2K) products; Global Modeling and Assimilation Office, NASA GES DISC).

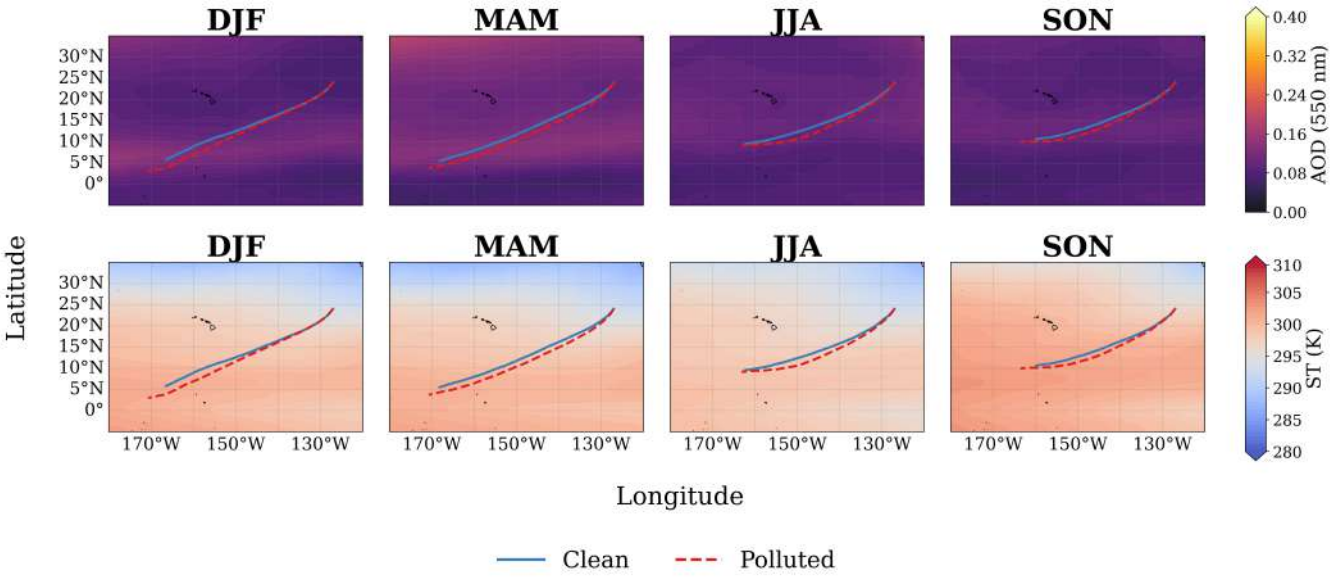

Figure S29. Seasonal mean AOD and sea surface (ST) environments for the NEP3 initial location (24.0°N, 127.0°W) trajectories, separated into clean (blue) and polluted (red, dashed) groups. The top row shows the seasonal mean AOD at 550 nm, and the bottom row shows the corresponding seasonal mean SST for each season (DJF, MAM, JJA, SON). Data from MERRA-2 reanalysis data (M2TMNXAER (DOI: (10.5067/FH9A0MLJPC7N) and M2TMNXSLV (DOI: 10.5067/AP1B0BA5PD2K) products; Global Modeling and Assimilation Office, NASA GES DISC).

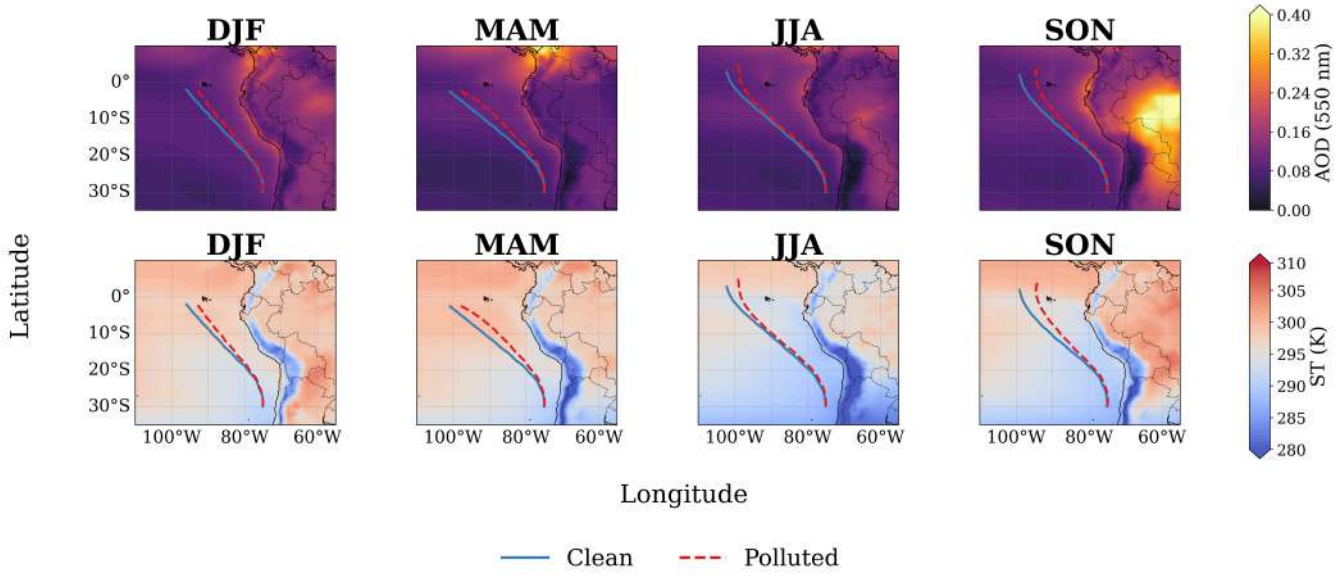

Figure S30. Seasonal mean AOD and sea surface (ST) environments for the SEP1 initial location (30.0°S, 75.0°W) trajectories, separated into clean (blue) and polluted (red, dashed) groups. The top row shows the seasonal mean AOD at 550 nm, and the bottom row shows the corresponding seasonal mean SST for each season (DJF, MAM, JJA, SON). Data from MERRA-2 reanalysis data (M2TMNXAER (DOI: (10.5067/FH9A0MLJPC7N) and M2TMNXSLV (DOI: 10.5067/AP1B0BA5PD2K) products; Global Modeling and Assimilation Office, NASA GES DISC).

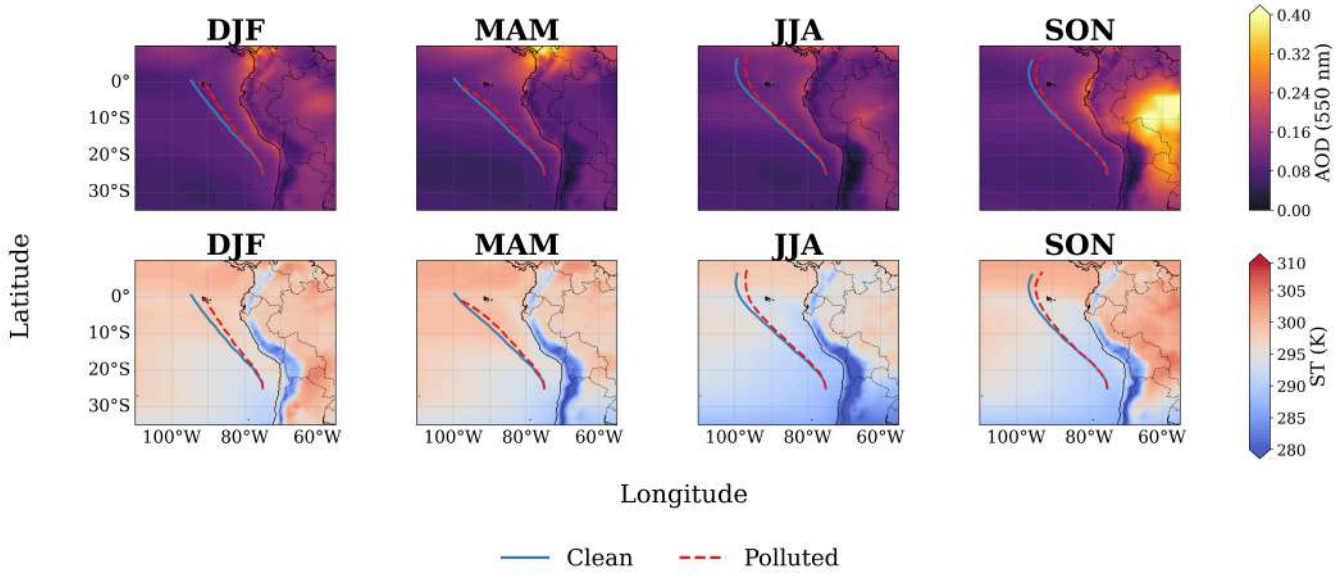

Figure S31. Seasonal mean AOD and sea surface (ST) environments for the SEP2 initial location (25.0°S, 75.0°W) trajectories, separated into clean (blue) and polluted (red, dashed) groups. The top row shows the seasonal mean AOD at 550 nm, and the bottom row shows the corresponding seasonal mean SST for each season (DJF, MAM, JJA, SON). Data from MERRA-2 reanalysis data (M2TMNXAER (DOI: (10.5067/FH9A0MLJPC7N) and M2TMNXSLV (DOI: 10.5067/AP1B0BA5PD2K) products; Global Modeling and Assimilation Office, NASA GES DISC).

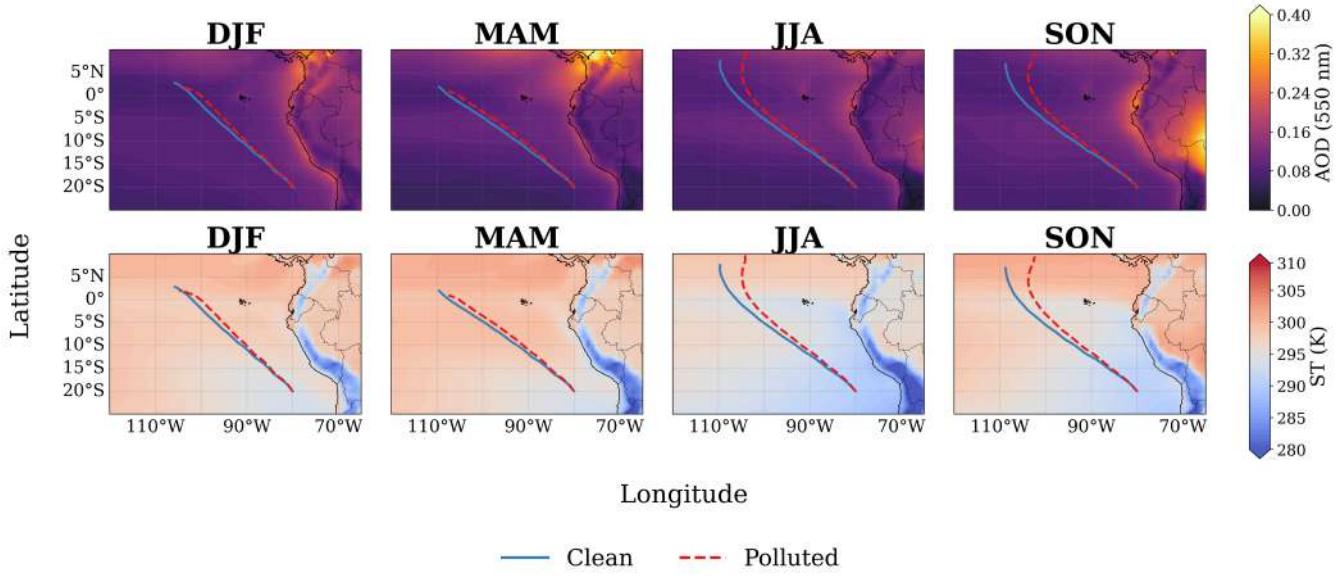

Figure S32. Seasonal mean AOD and sea surface (ST) environments for the SEP3 initial location (20.0°S, 80.0°W) trajectories, separated into clean (blue) and polluted (red, dashed) groups. The top row shows the seasonal mean AOD at 550 nm, and the bottom row shows the corresponding seasonal mean SST for each season (DJF, MAM, JJA, SON). Data from MERRA-2 reanalysis data (M2TMNXAER (DOI: (10.5067/FH9A0MLJPC7N) and M2TMNXSLV (DOI: 10.5067/AP1B0BA5PD2K) products; Global Modeling and Assimilation Office, NASA GES DISC).

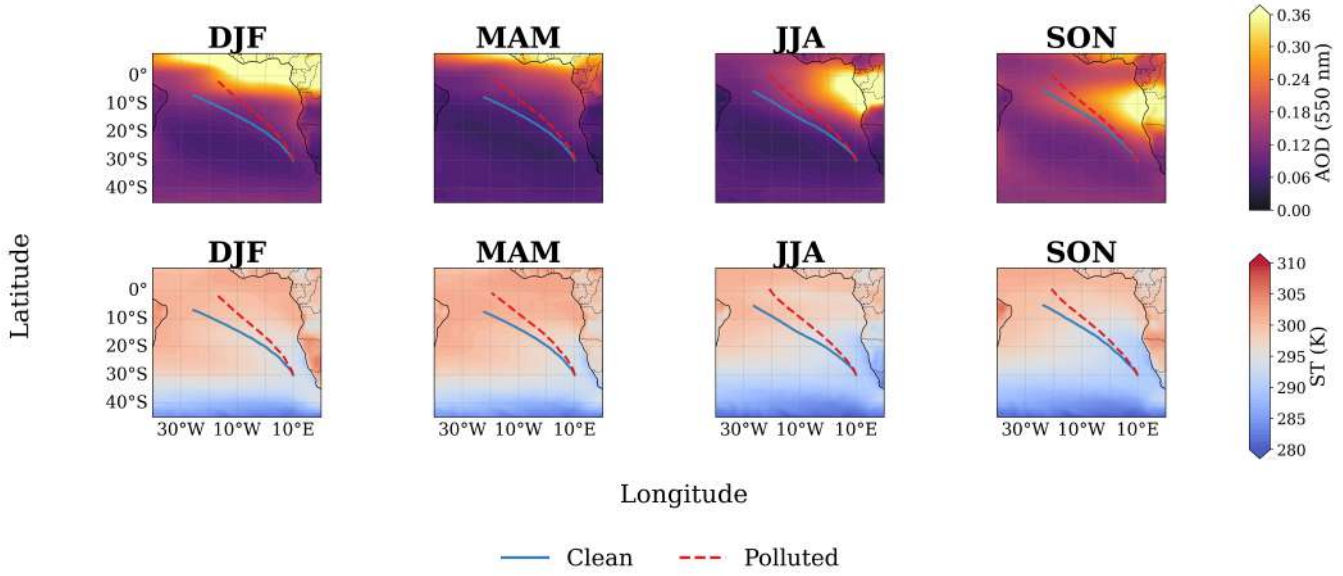

Figure S33. Seasonal mean AOD and sea surface (ST) environments for the SEA1 initial location (30.0°S, 10.0°E) trajectories, separated into clean (blue) and polluted (red, dashed) groups. The top row shows the seasonal mean AOD at 550 nm, and the bottom row shows the corresponding seasonal mean SST for each season (DJF, MAM, JJA, SON). Data from MERRA-2 reanalysis data (M2TMNXAER (DOI: (10.5067/FH9A0MLJPC7N) and M2TMNXSLV (DOI: 10.5067/AP1B0BA5PD2K) products; Global Modeling and Assimilation Office, NASA GES DISC).

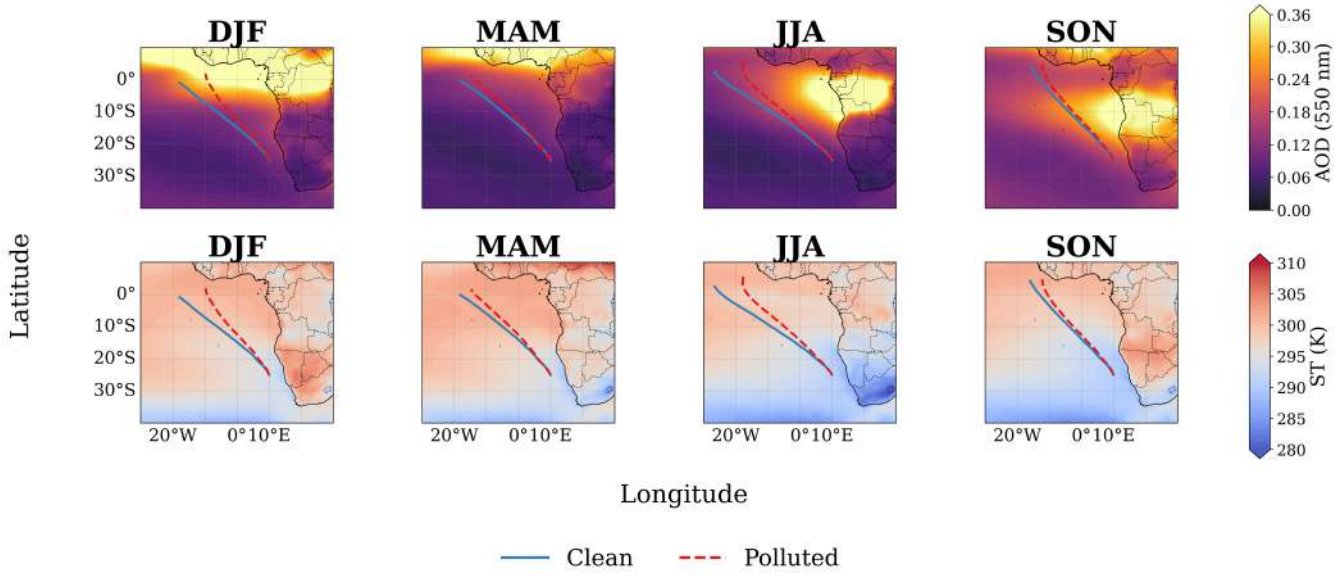

Figure S34. Seasonal mean AOD and sea surface (ST) environments for the SEA2 initial location (25.0°S, 10.0°E) trajectories, separated into clean (blue) and polluted (red, dashed) groups. The top row shows the seasonal mean AOD at 550 nm, and the bottom row shows the corresponding seasonal mean SST for each season (DJF, MAM, JJA, SON). Data from MERRA-2 reanalysis data (M2TMNXAER (DOI: (10.5067/FH9A0MLJPC7N) and M2TMNXSLV (DOI: 10.5067/AP1B0BA5PD2K) products; Global Modeling and Assimilation Office, NASA GES DISC).

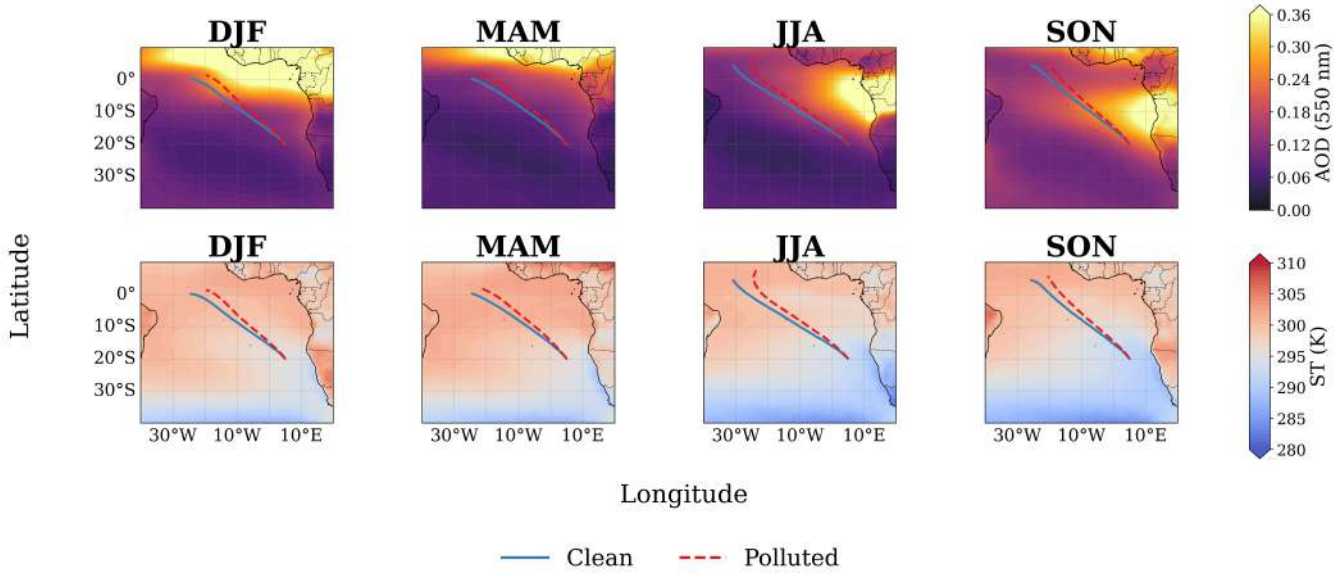

Figure S35. Seasonal mean AOD and sea surface (ST) environments for the SEA3 initial location (20.0°S, 5.0°E) trajectories, separated into clean (blue) and polluted (red, dashed) groups. The top row shows the seasonal mean AOD at 550 nm, and the bottom row shows the corresponding seasonal mean SST for each season (DJF, MAM, JJA, SON). Data from MERRA-2 reanalysis data (M2TMNXAER (DOI: (10.5067/FH9A0MLJPC7N) and M2TMNXSLV (DOI: 10.5067/AP1B0BA5PD2K) products; Global Modeling and Assimilation Office, NASA GES DISC).

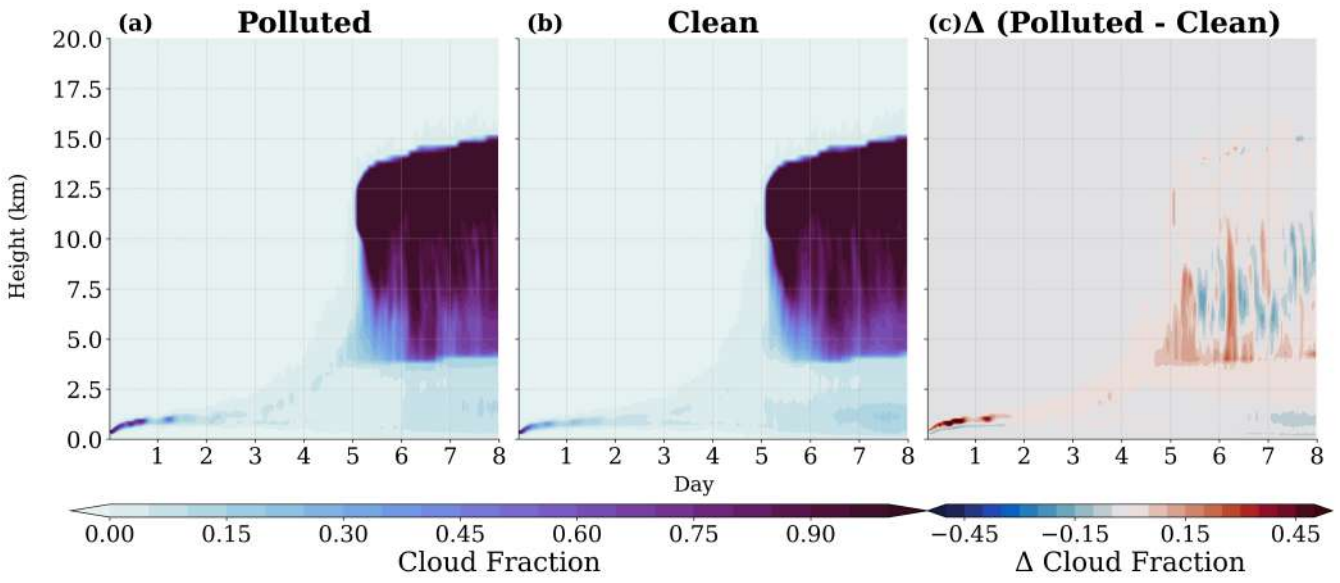

Figure S36. Hovmöller diagrams of cloud fraction evolution from model simulations for the NEP2 initial location (28.0°N, 121.0°W), for the different simulated cases: (a) polluted simulation, (b) clean simulation, and (c) the difference between them (polluted − clean). Panels (a) and (b) show cloud fraction as a function of height and time, while panel (c) shows the corresponding difference field. Color scales for cloud fraction and surface temperature are shown alongside each plot.

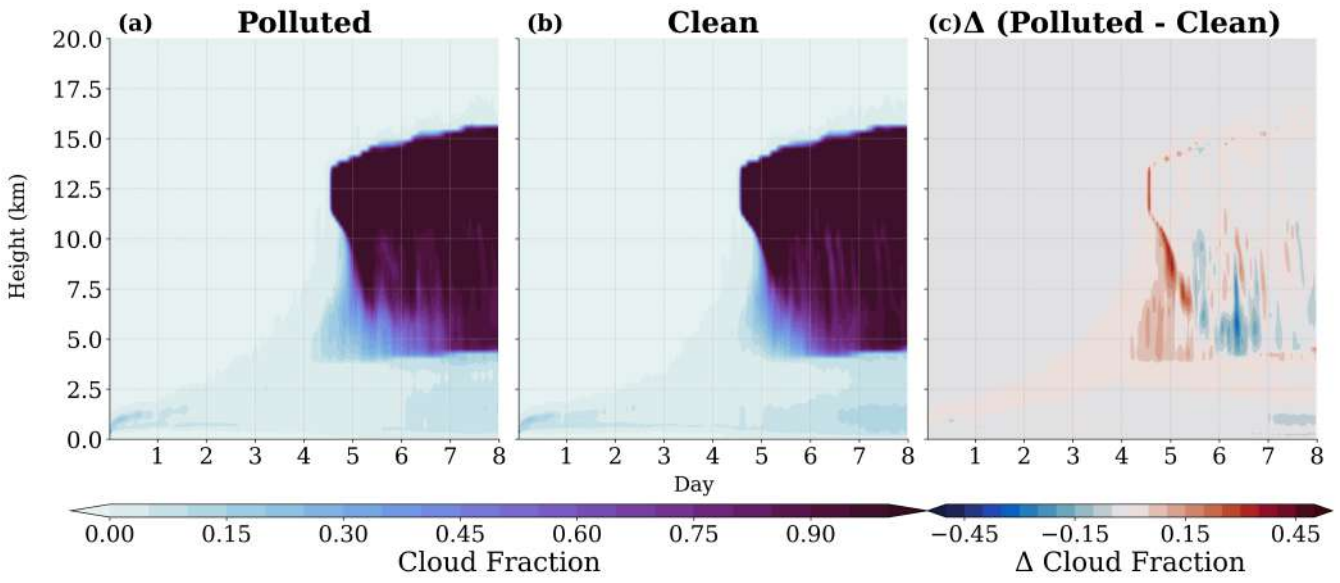

Figure S37. Hovmöller diagrams of cloud fraction evolution from model simulations for the NEP3 initial location (24.0°N, 127.0°W), for the different simulated cases: (a) polluted simulation, (b) clean simulation, and (c) the difference between them (polluted − clean). Panels (a) and (b) show cloud fraction as a function of height and time, while panel (c) shows the corresponding difference field. Color scales for cloud fraction and surface temperature are shown alongside each plot.

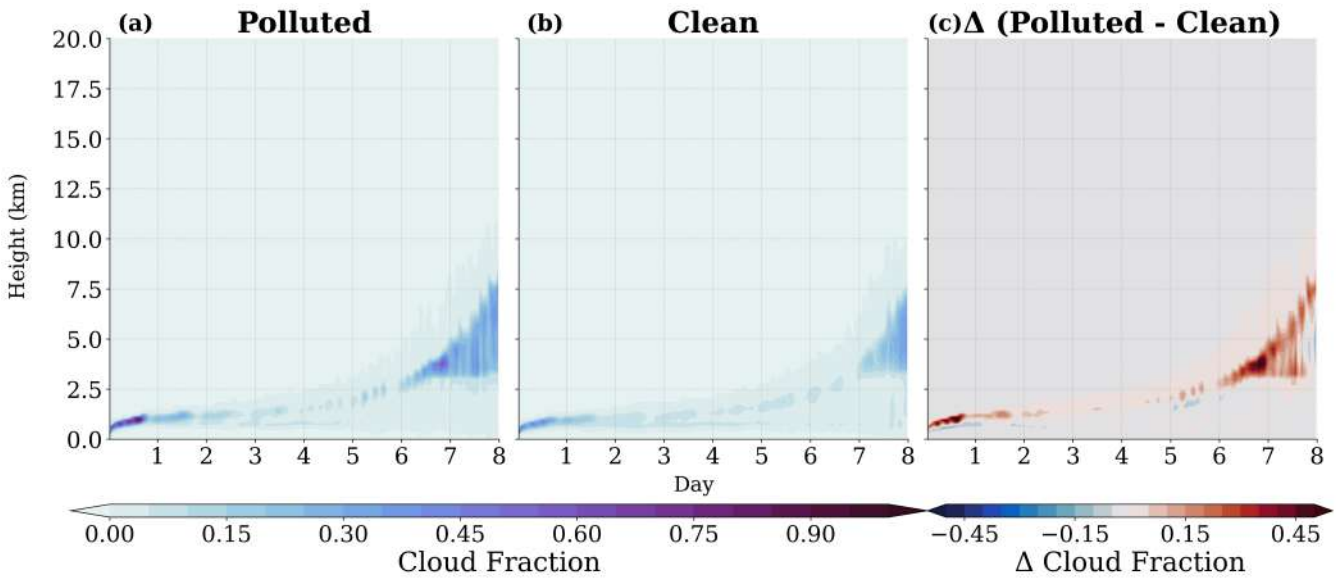

Figure S38. Hovmöller diagrams of cloud fraction evolution from model simulations for the SEP1 initial location (30.0°S, 75.0°W), for the different simulated cases: (a) polluted simulation, (b) clean simulation, and (c) the difference between them (polluted − clean). Panels (a) and (b) show cloud fraction as a function of height and time, while panel (c) shows the corresponding difference field. Color scales for cloud fraction and surface temperature are shown alongside each plot.

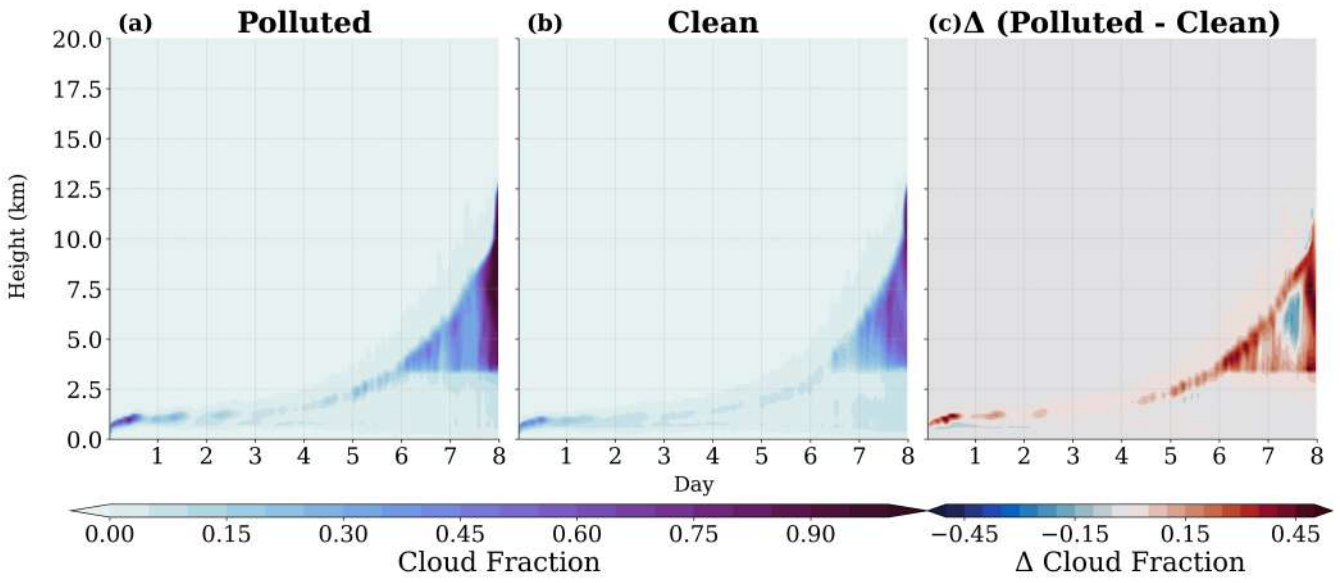

Figure S39. Hovmöller diagrams of cloud fraction evolution from model simulations for the SEP2 initial location (25.0°S, 75.0°W), for the different simulated cases: (a) polluted simulation, (b) clean simulation, and (c) the difference between them (polluted − clean). Panels (a) and (b) show cloud fraction as a function of height and time, while panel (c) shows the corresponding difference field. Color scales for cloud fraction and surface temperature are shown alongside each plot.

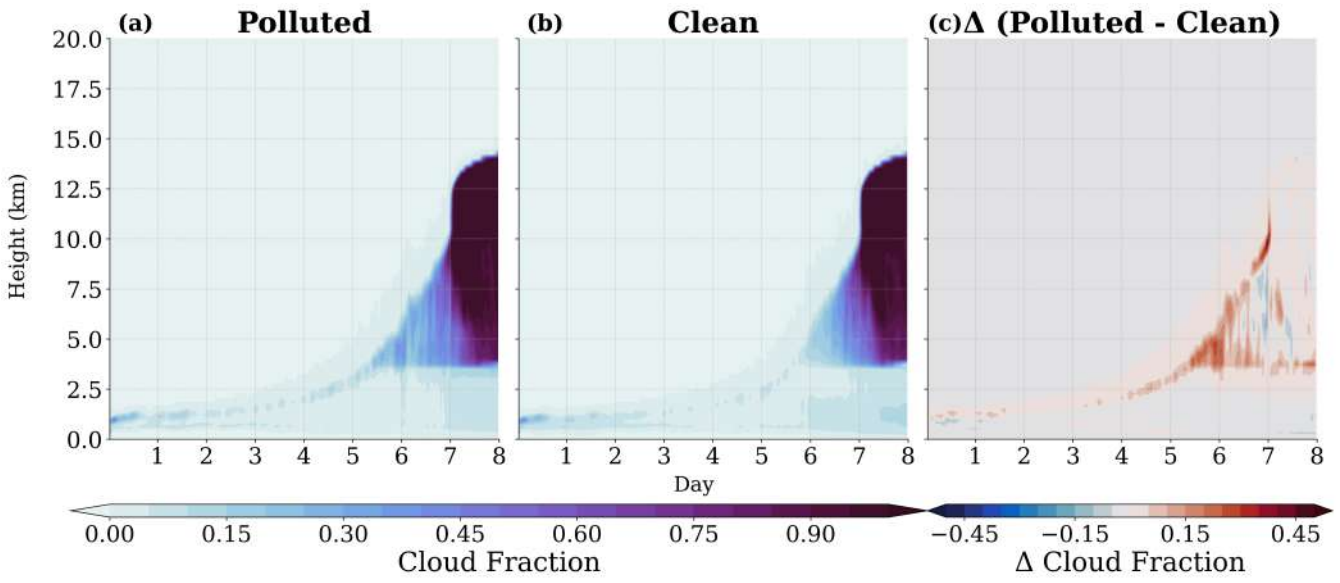

Figure S40. Hovmöller diagrams of cloud fraction evolution from model simulations for the SEP3 initial location (20.0°S, 80.0°W), for the different simulated cases: (a) polluted simulation, (b) clean simulation, and (c) the difference between them (polluted − clean). Panels (a) and (b) show cloud fraction as a function of height and time, while panel (c) shows the corresponding difference field. Color scales for cloud fraction and surface temperature are shown alongside each plot.

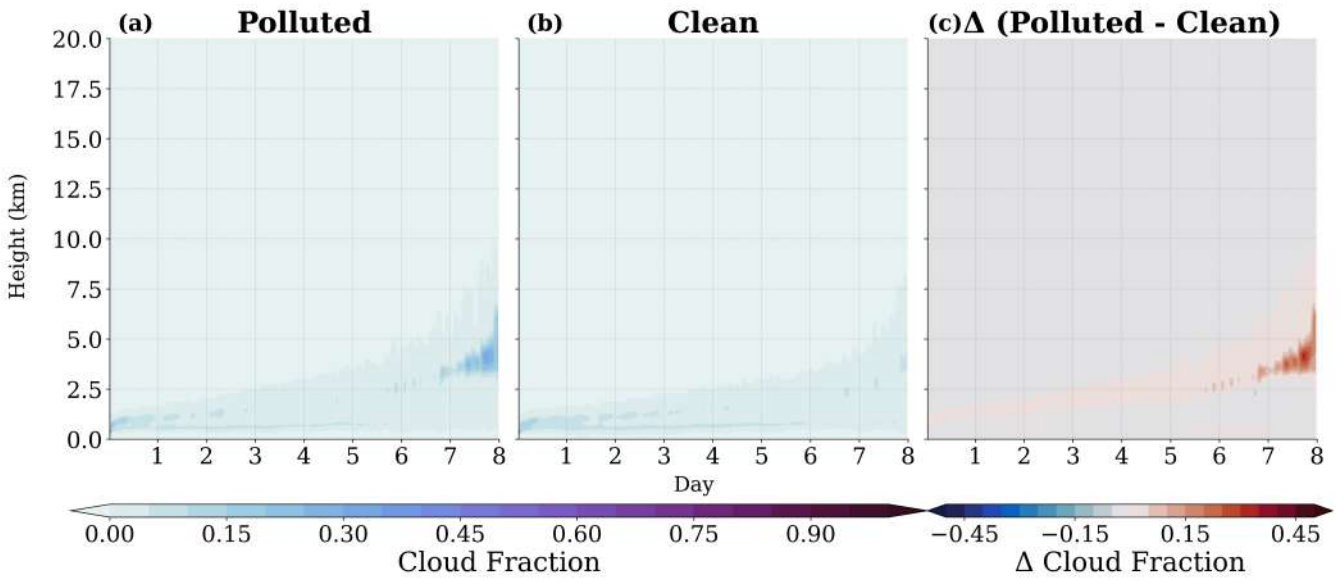

Figure S41. Hovmöller diagrams of cloud fraction evolution from model simulations for the SEA1 initial location (30.0°S, 10.0°E), for the different simulated cases: (a) polluted simulation, (b) clean simulation, and (c) the difference between them (polluted − clean). Panels (a) and (b) show cloud fraction as a function of height and time, while panel (c) shows the corresponding difference field. Color scales for cloud fraction and surface temperature are shown alongside each plot.

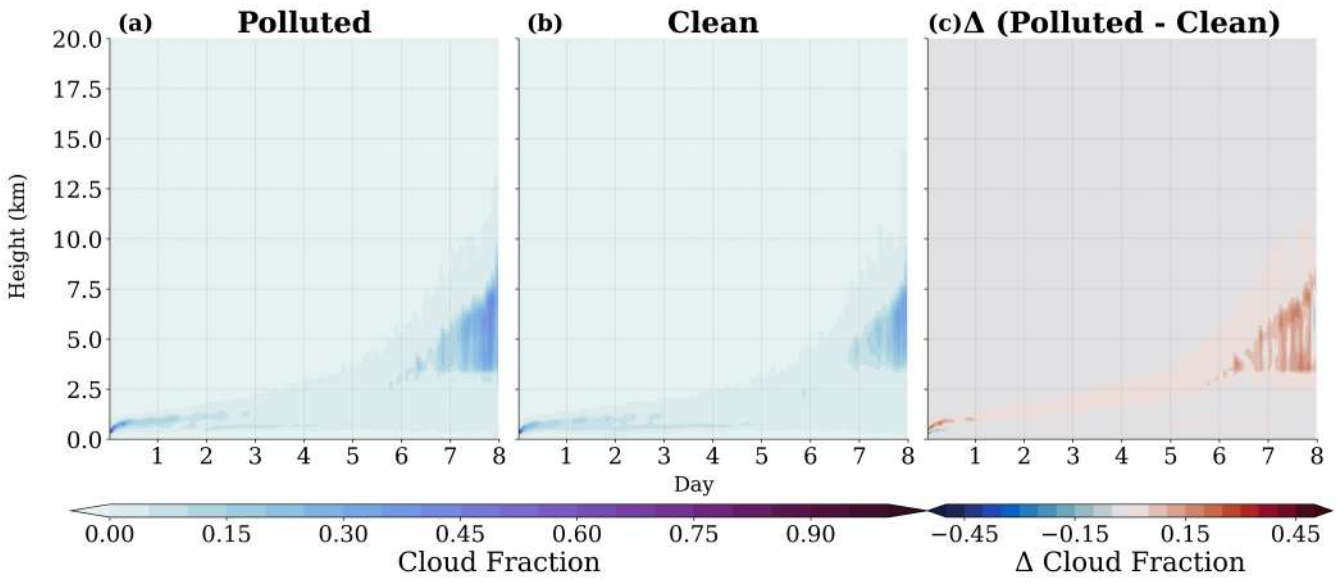

Figure S42. Hovmöller diagrams of cloud fraction evolution from model simulations for the SEA2 initial location (25.0°S, 10.0°E), for the different simulated cases: (a) polluted simulation, (b) clean simulation, and (c) the difference between them (polluted − clean). Panels (a) and (b) show cloud fraction as a function of height and time, while panel (c) shows the corresponding difference field. Color scales for cloud fraction and surface temperature are shown alongside each plot.

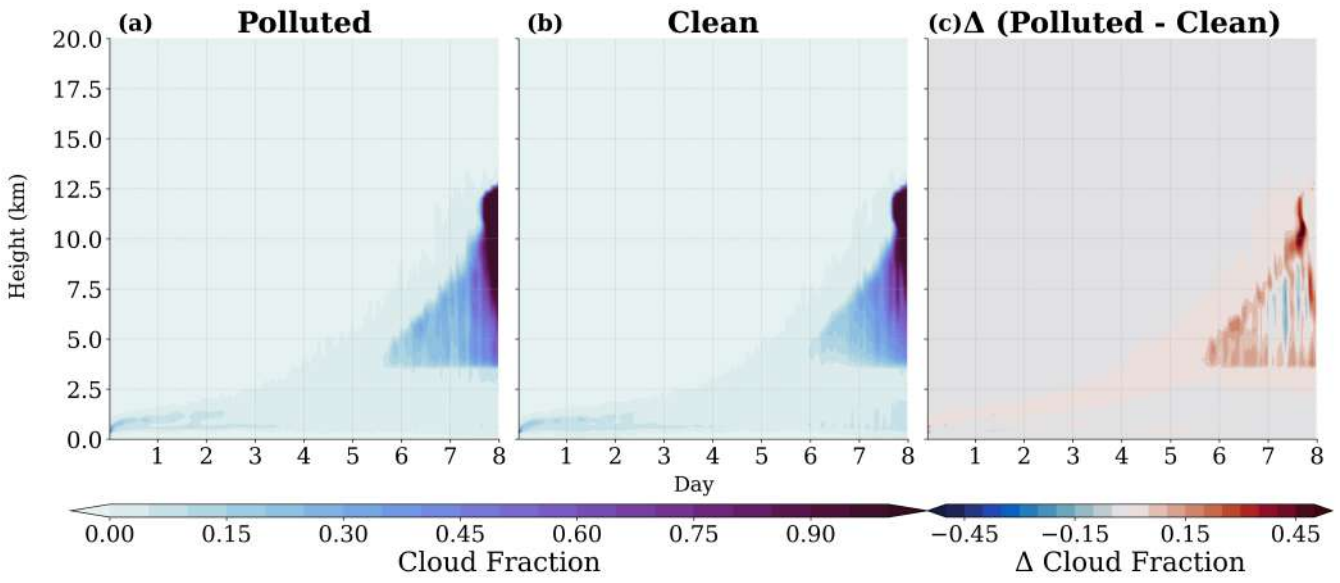

Figure S43. Hovmöller diagrams of cloud fraction evolution from model simulations for the SEA3 initial location (20.0°S, 5.0°E), for the different simulated cases: (a) polluted simulation, (b) clean simulation, and (c) the difference between them (polluted − clean). Panels (a) and (b) show cloud fraction as a function of height and time, while panel (c) shows the corresponding difference field. Color scales for cloud fraction and surface temperature are shown alongside each plot.

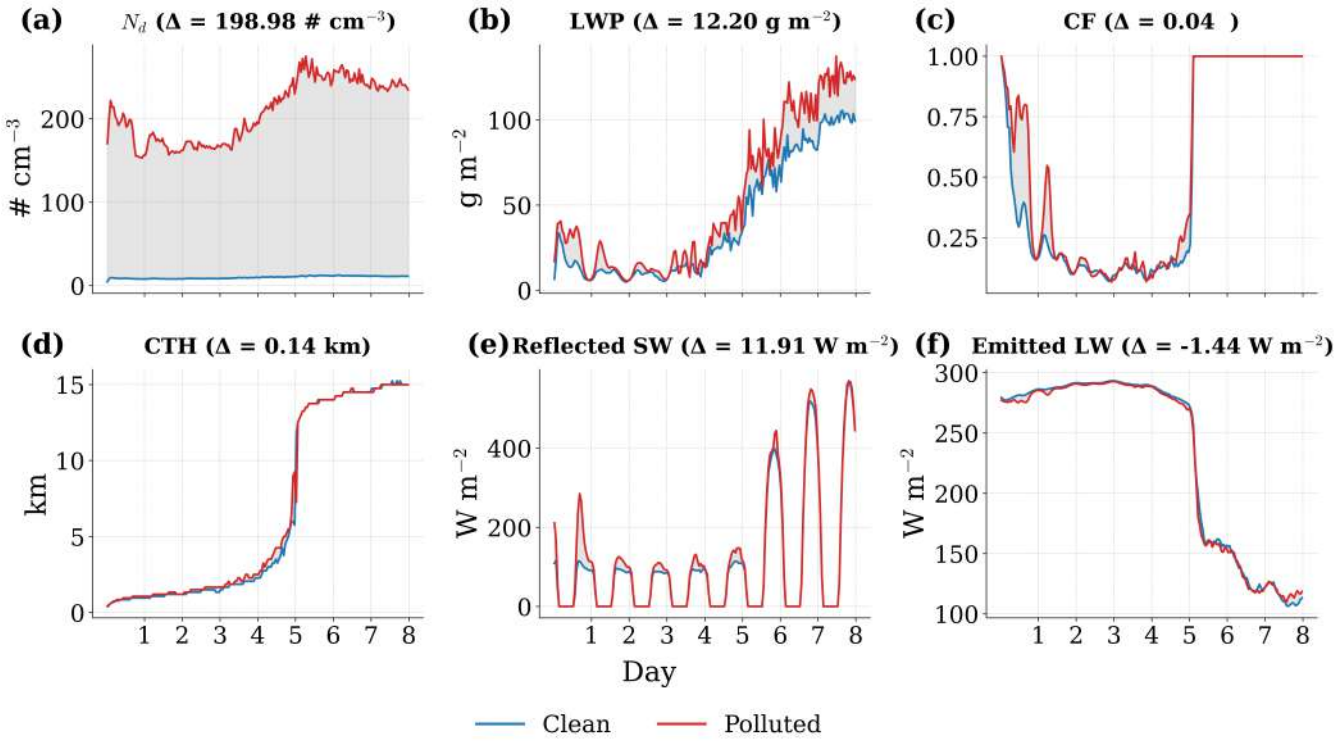

Figure S44. Hourly mean evolution of cloud and radiation variables from the model simulation for the NEP2 initial location (28.0°N, 121.0°W), separated into clean (blue; 20cm^{-3}) and polluted (red; 800cm^{-3}) groups. Panels show: (a) Domain mean cloud droplet number concentration (N_d), (b) liquid water path (LWP), (c) total cloud fraction (CF), (d) cloud top height (CTH), (e) reflected shortwave radiation at top of atmosphere (TOA; Reflected SW), (f) emitted longwave radiation at TOA (Emitted LW). The time-mean differences between the polluted and clean simulations are shown in parentheses above each panel.

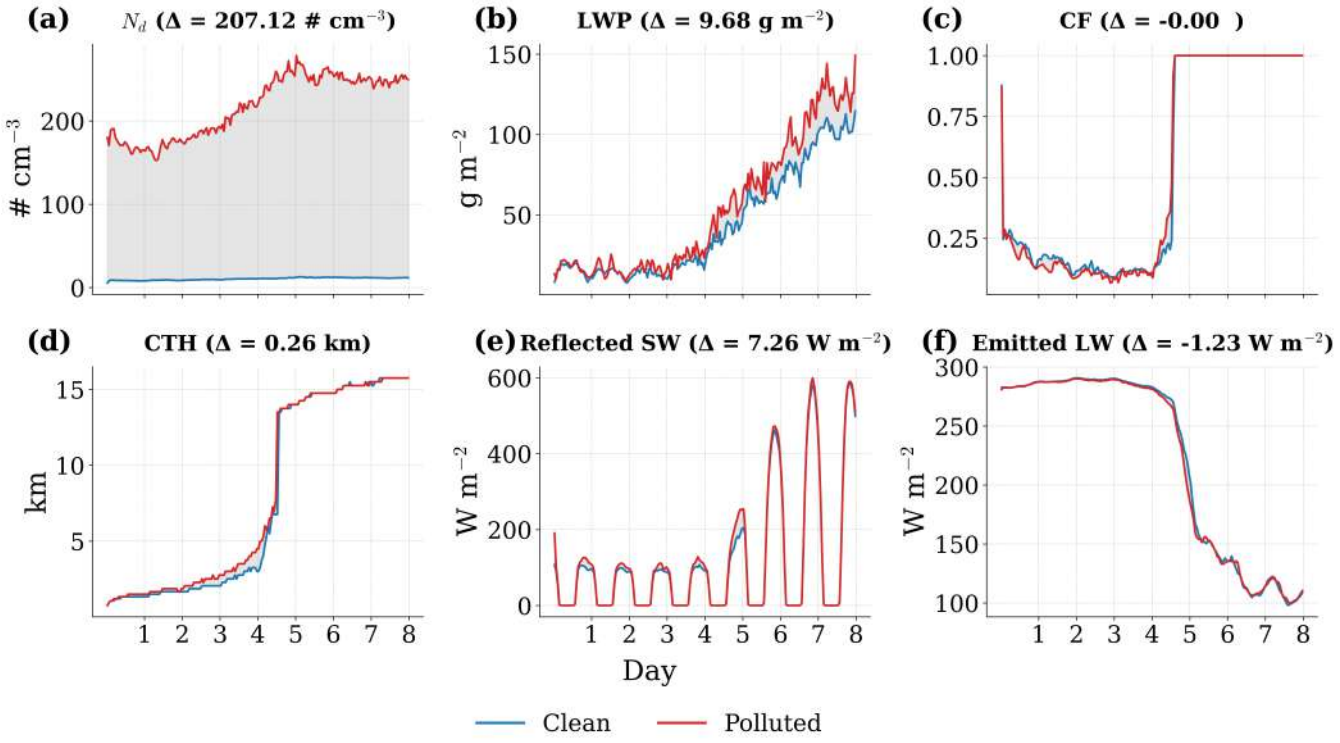

Figure S45. Hourly mean evolution of cloud and radiation variables from the model simulation for the NEP3 initial location (24.0°N, 127.0°W), separated into clean (blue; 20cm^{-3}) and polluted (red; 800cm^{-3}) groups. Panels show: (a) Domain mean cloud droplet number concentration (N_d), (b) liquid water path (LWP), (c) total cloud fraction (CF), (d) cloud top height (CTH), (e) reflected shortwave radiation at top of atmosphere (TOA; Reflected SW), (f) emitted longwave radiation at TOA (Emitted LW). The time-mean differences between the polluted and clean simulations are shown in parentheses above each panel.

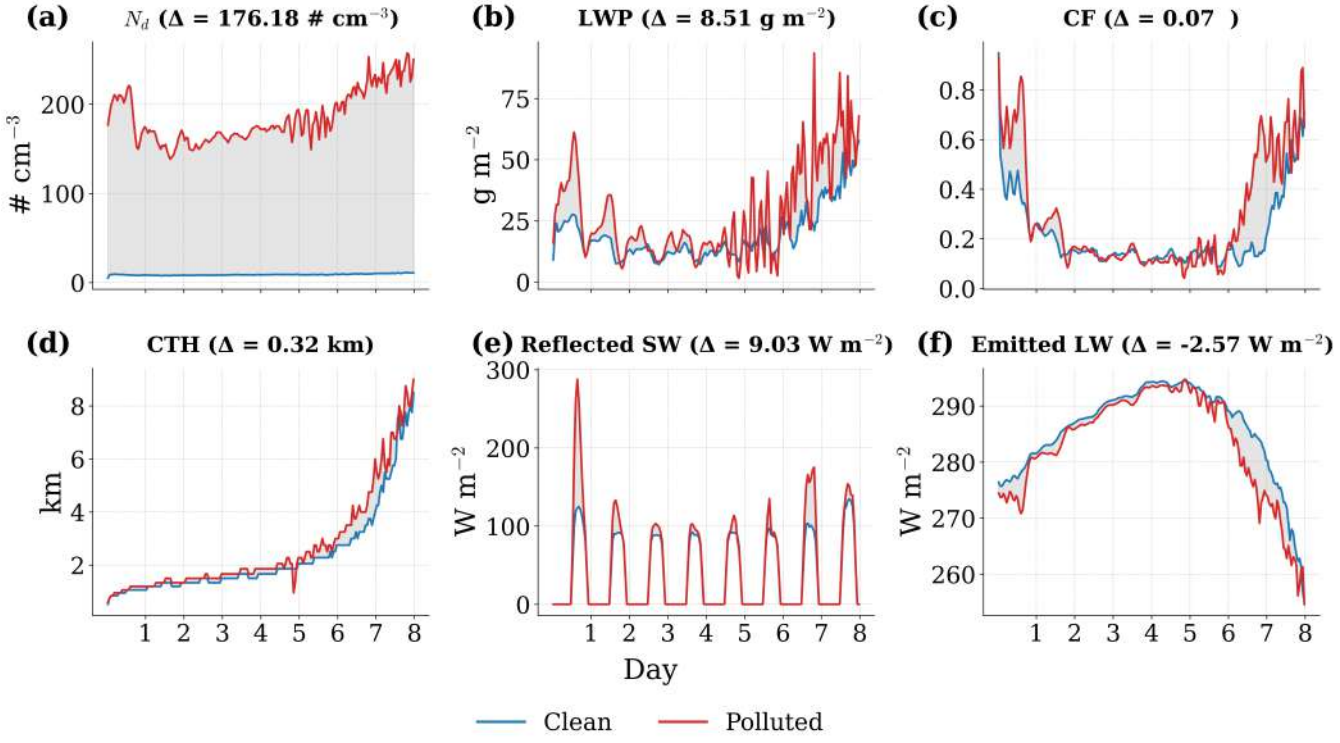

Figure S46. Hourly mean evolution of cloud and radiation variables from the model simulation for the SEP1 initial location (30.0°S, 75.0°W), separated into clean (blue; 20cm^{-3}) and polluted (red; 800cm^{-3}) groups. Panels show: (a) Domain mean cloud droplet number concentration (N_d), (b) liquid water path (LWP), (c) total cloud fraction (CF), (d) cloud top height (CTH), (e) reflected shortwave radiation at top of atmosphere (TOA; Reflected SW), (f) emitted longwave radiation at TOA (Emitted LW). The time-mean differences between the polluted and clean simulations are shown in parentheses above each panel.

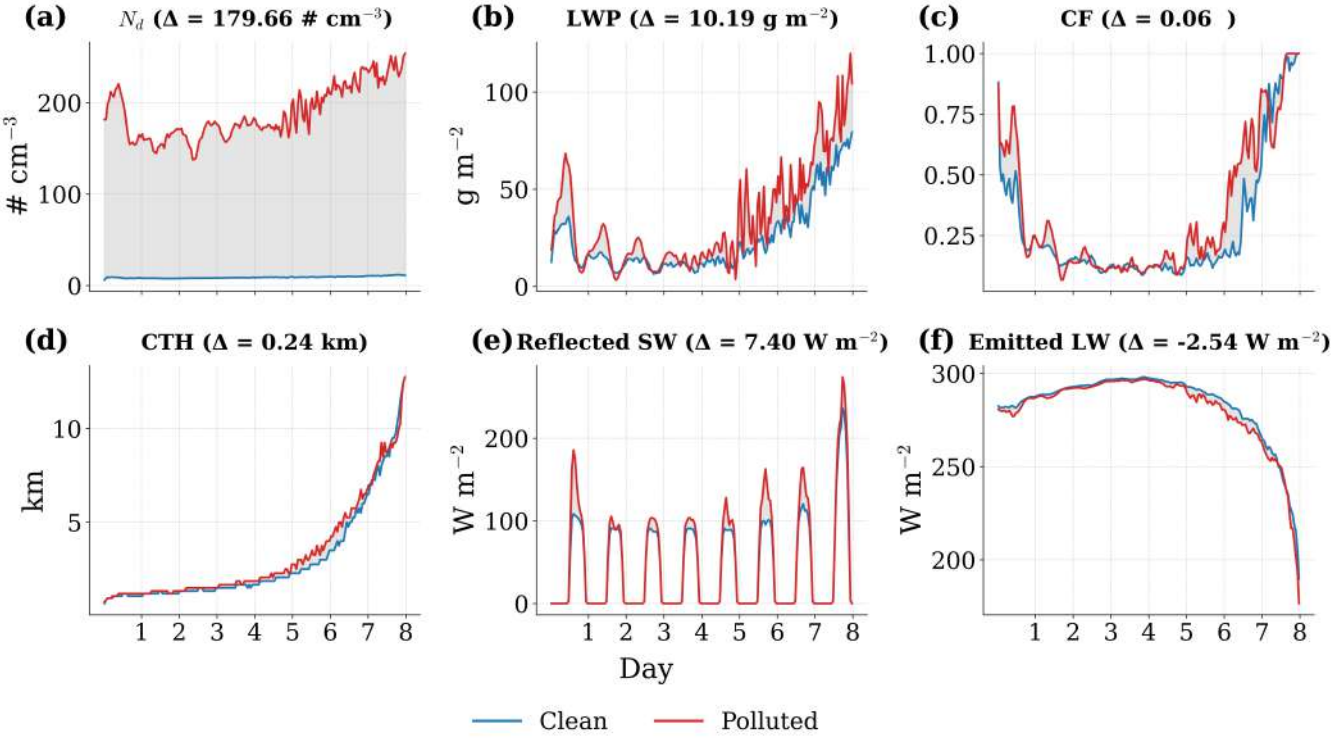

Figure S47. Hourly mean evolution of cloud and radiation variables from the model simulation for the SEP2 initial location (25.0°S, 75.0°W), separated into clean (blue; 20cm^{-3}) and polluted (red; 800cm^{-3}) groups. Panels show: (a) Domain mean cloud droplet number concentration (N_d), (b) liquid water path (LWP), (c) total cloud fraction (CF), (d) cloud top height (CTH), (e) reflected shortwave radiation at top of atmosphere (TOA; Reflected SW), (f) emitted longwave radiation at TOA (Emitted LW). The time-mean differences between the polluted and clean simulations are shown in parentheses above each panel.

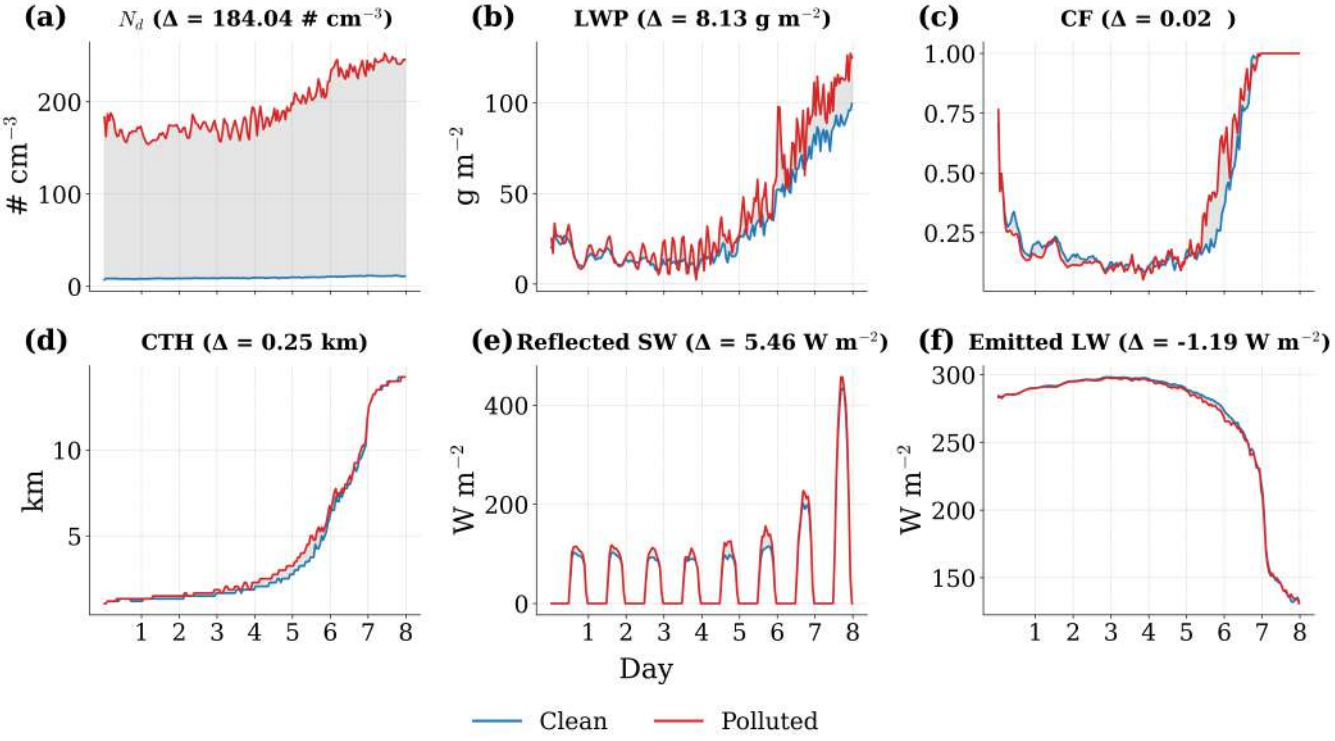

Figure S48. Hourly mean evolution of cloud and radiation variables from the model simulation for the SEP3 initial location (20.0°S, 80.0°W), separated into clean (blue; 20cm^{-3}) and polluted (red; 800cm^{-3}) groups. Panels show: (a) Domain mean cloud droplet number concentration (N_d), (b) liquid water path (LWP), (c) total cloud fraction (CF), (d) cloud top height (CTH), (e) reflected shortwave radiation at top of atmosphere (TOA; Reflected SW), (f) emitted longwave radiation at TOA (Emitted LW). The time-mean differences between the polluted and clean simulations are shown in parentheses above each panel.

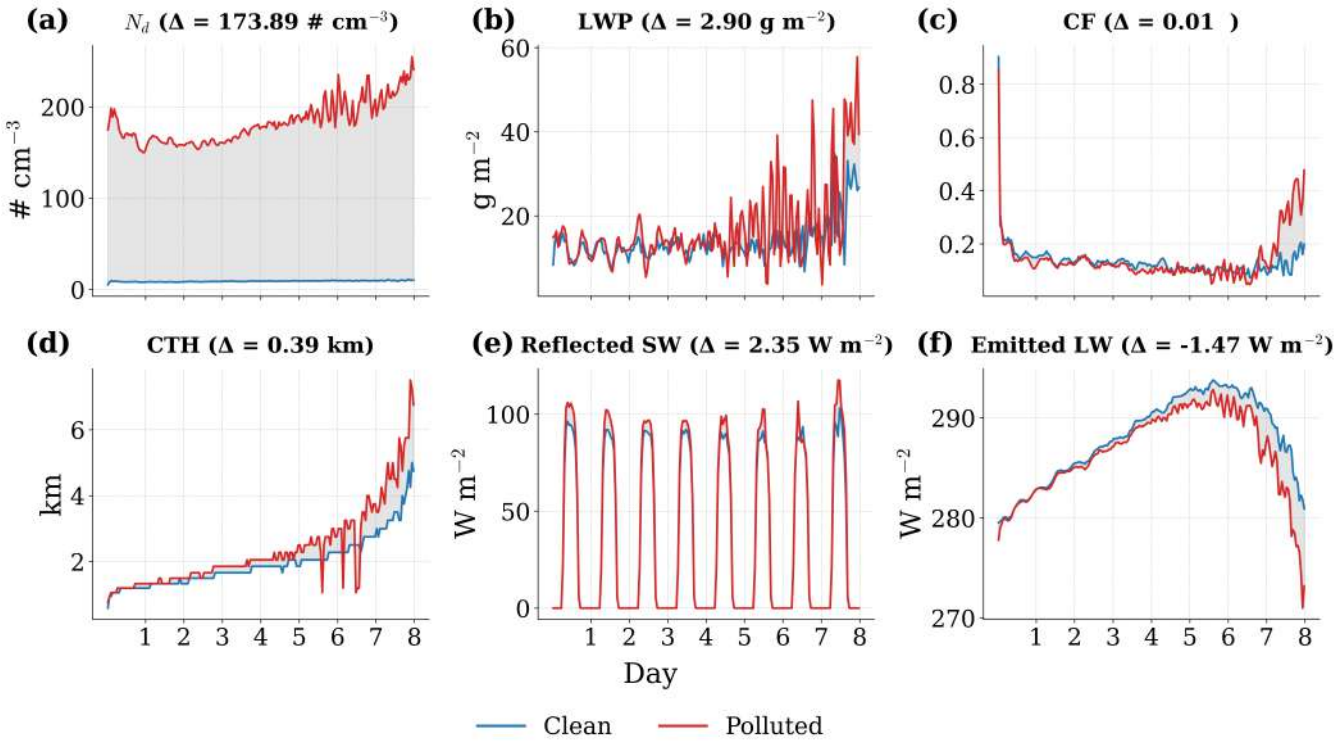

Figure S49. Hourly mean evolution of cloud and radiation variables from the model simulation for the SEA1 initial location (30.0°S, 10.0°E), separated into clean (blue; 20cm^{-3}) and polluted (red; 800cm^{-3}) groups. Panels show: (a) Domain mean cloud droplet number concentration (N_d), (b) liquid water path (LWP), (c) total cloud fraction (CF), (d) cloud top height (CTH), (e) reflected shortwave radiation at top of atmosphere (TOA; Reflected SW), (f) emitted longwave radiation at TOA (Emitted LW). The time-mean differences between the polluted and clean simulations are shown in parentheses above each panel.

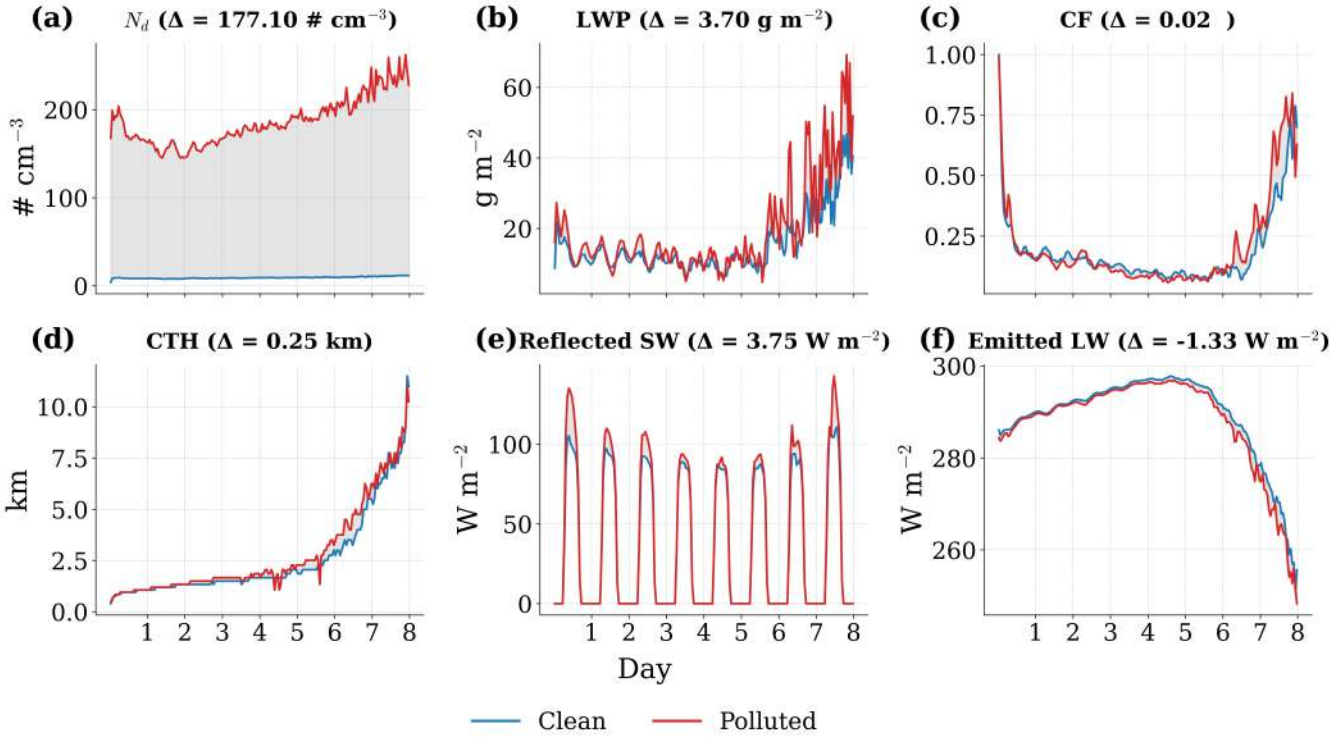

Figure S50. Hourly mean evolution of cloud and radiation variables from the model simulation for the SEA2 initial location (25.0°S, 10.0°E), separated into clean (blue; 20cm^{-3}) and polluted (red; 800cm^{-3}) groups. Panels show: (a) Domain mean cloud droplet number concentration (N_d), (b) liquid water path (LWP), (c) total cloud fraction (CF), (d) cloud top height (CTH), (e) reflected shortwave radiation at top of atmosphere (TOA; Reflected SW), (f) emitted longwave radiation at TOA (Emitted LW). The time-mean differences between the polluted and clean simulations are shown in parentheses above each panel.

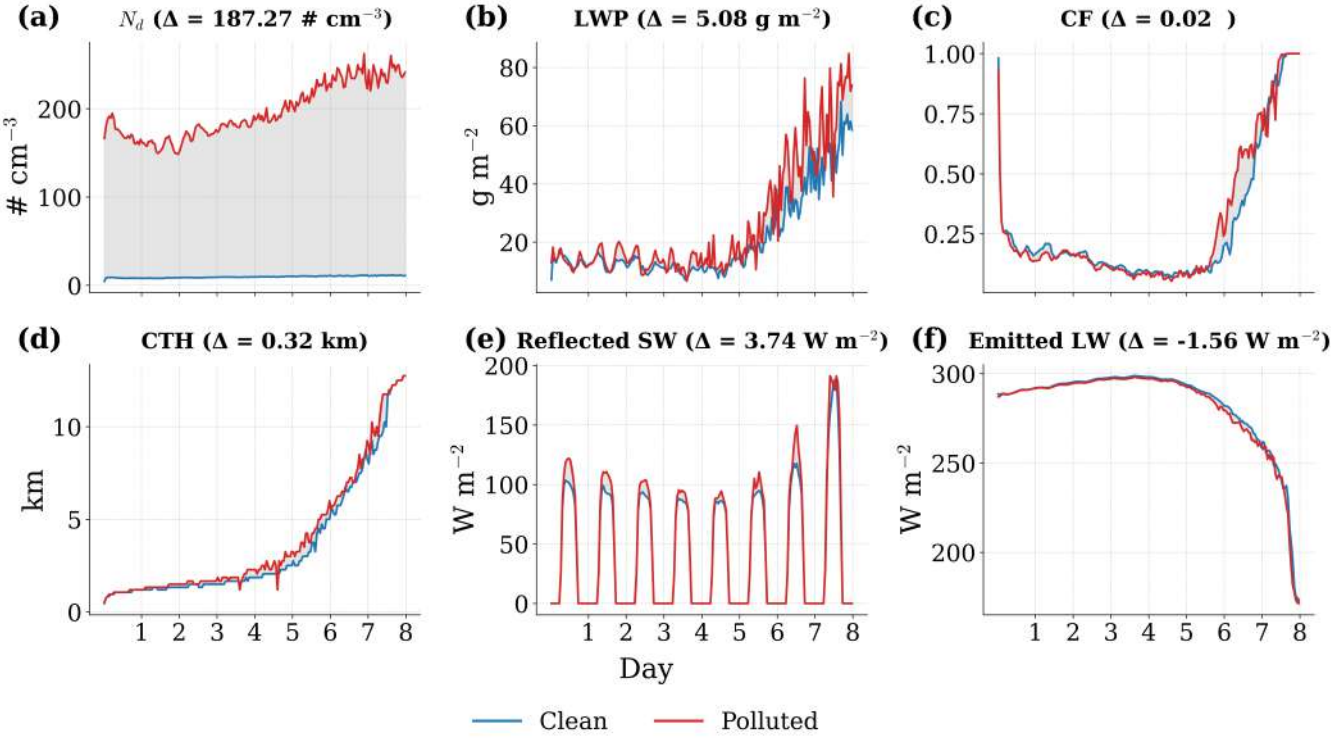

Figure S51. Hourly mean evolution of cloud and radiation variables from the model simulation for the SEA3 initial location (20.0°S, 5.0°E), separated into clean (blue; 20cm^{-3}) and polluted (red; 800cm^{-3}) groups. Panels show: (a) Domain mean cloud droplet number concentration (N_d), (b) liquid water path (LWP), (c) total cloud fraction (CF), (d) cloud top height (CTH), (e) reflected shortwave radiation at top of atmosphere (TOA; Reflected SW), (f) emitted longwave radiation at TOA (Emitted LW). The time-mean differences between the polluted and clean simulations are shown in parentheses above each panel.

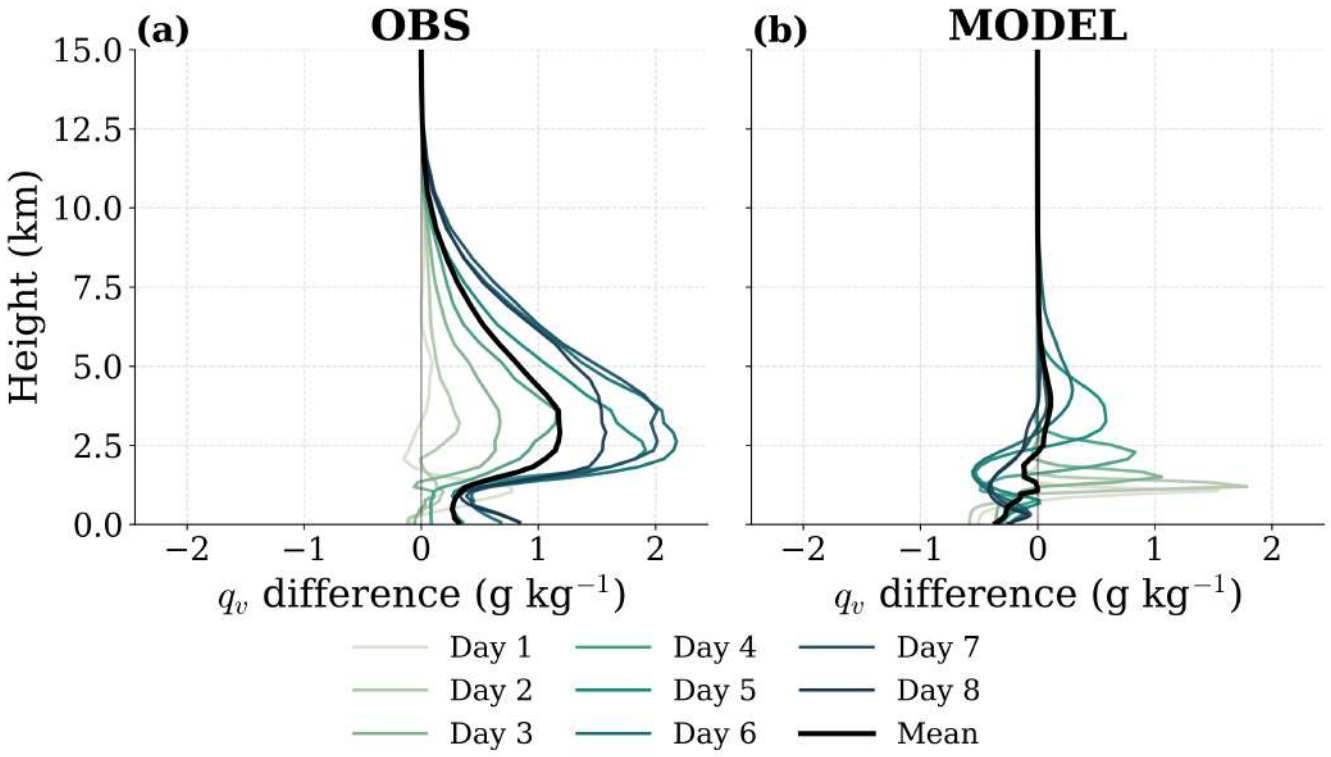

Figure S52. Daily (colors) and time-mean differences (black) in the vertical profile of specific humidity (q_v) between polluted and clean conditions from observations (panel a) and model simulations (panel b) at NEP2 (28.0°N, 121.0°W).

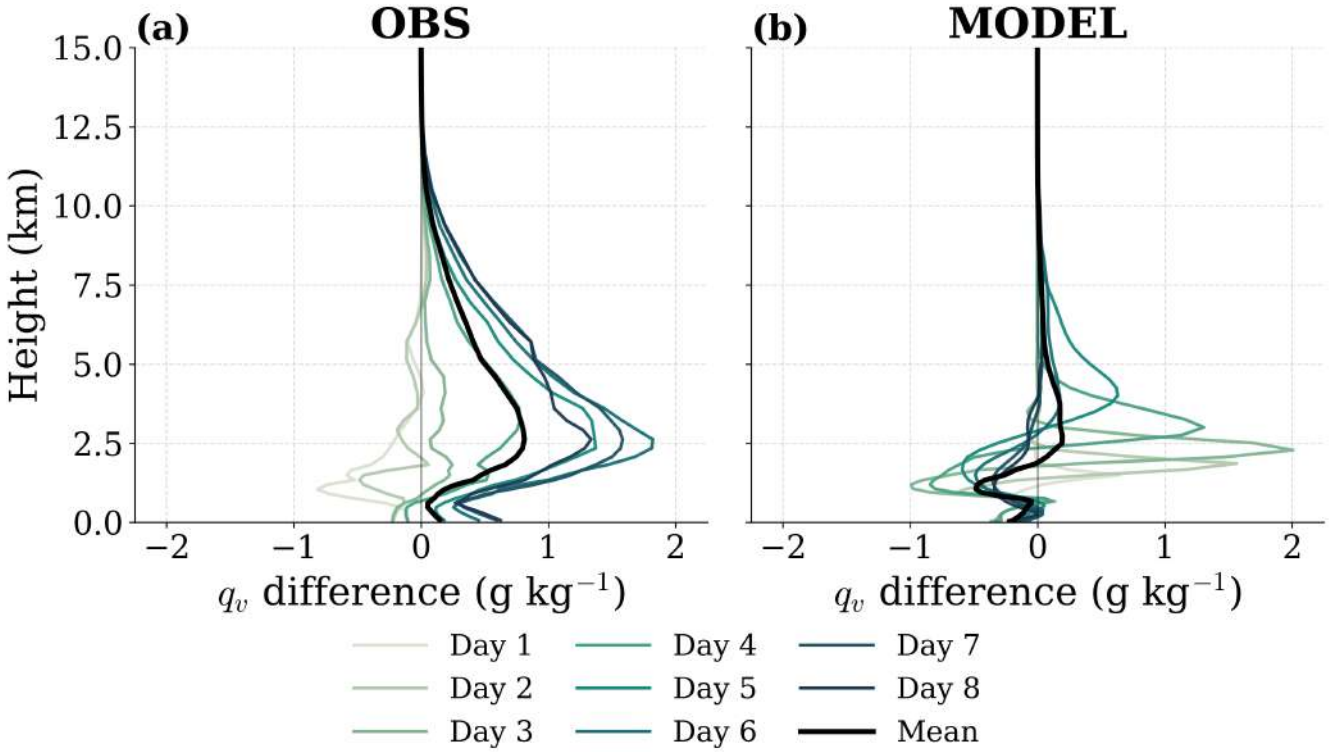

Figure S53. Daily (colors) and time-mean differences (black) in the vertical profile of specific humidity (q_v) between polluted and clean conditions from observations (panel a) and model simulations (panel b) at NEP3 (24.0°N, 127.0°W).

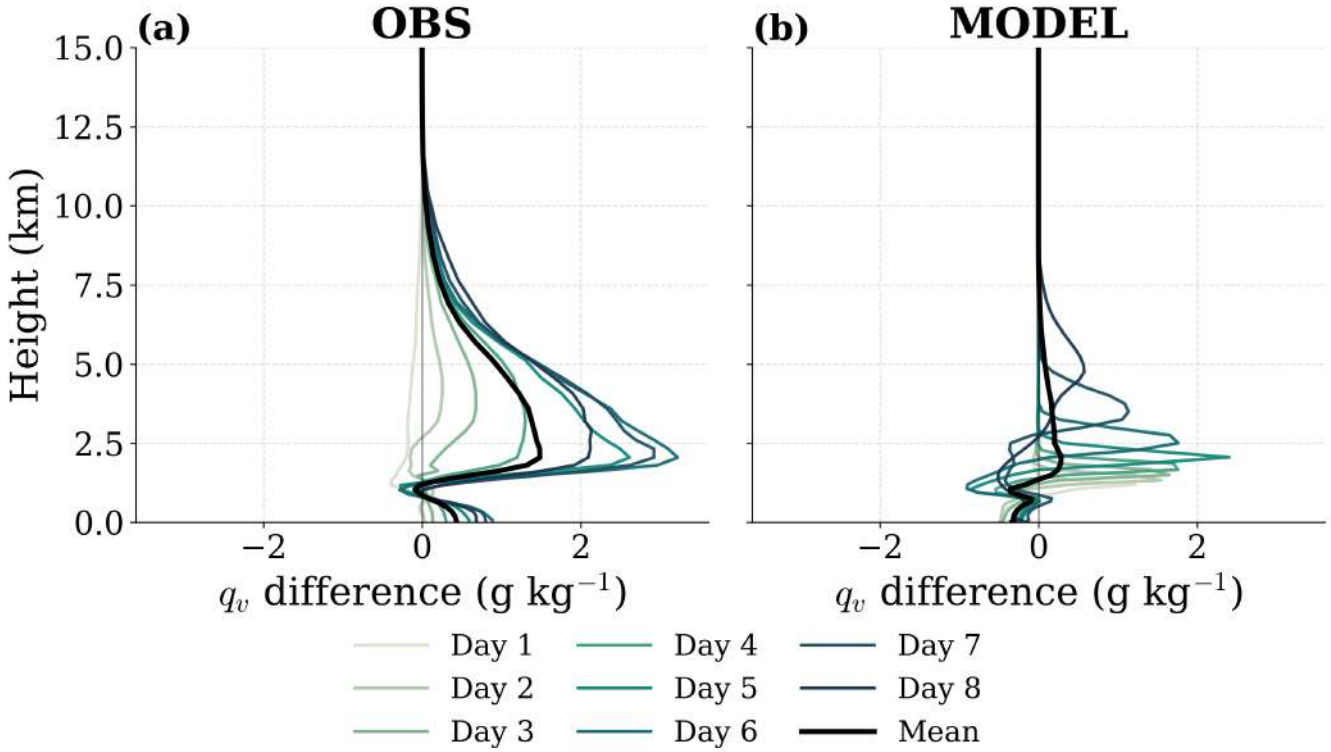

Figure S54. Daily (colors) and time-mean differences (black) in the vertical profile of specific humidity (q_v) between polluted and clean conditions from observations (panel a) and model simulations (panel b) at SEP1 (30.0°S, 75.0°W).

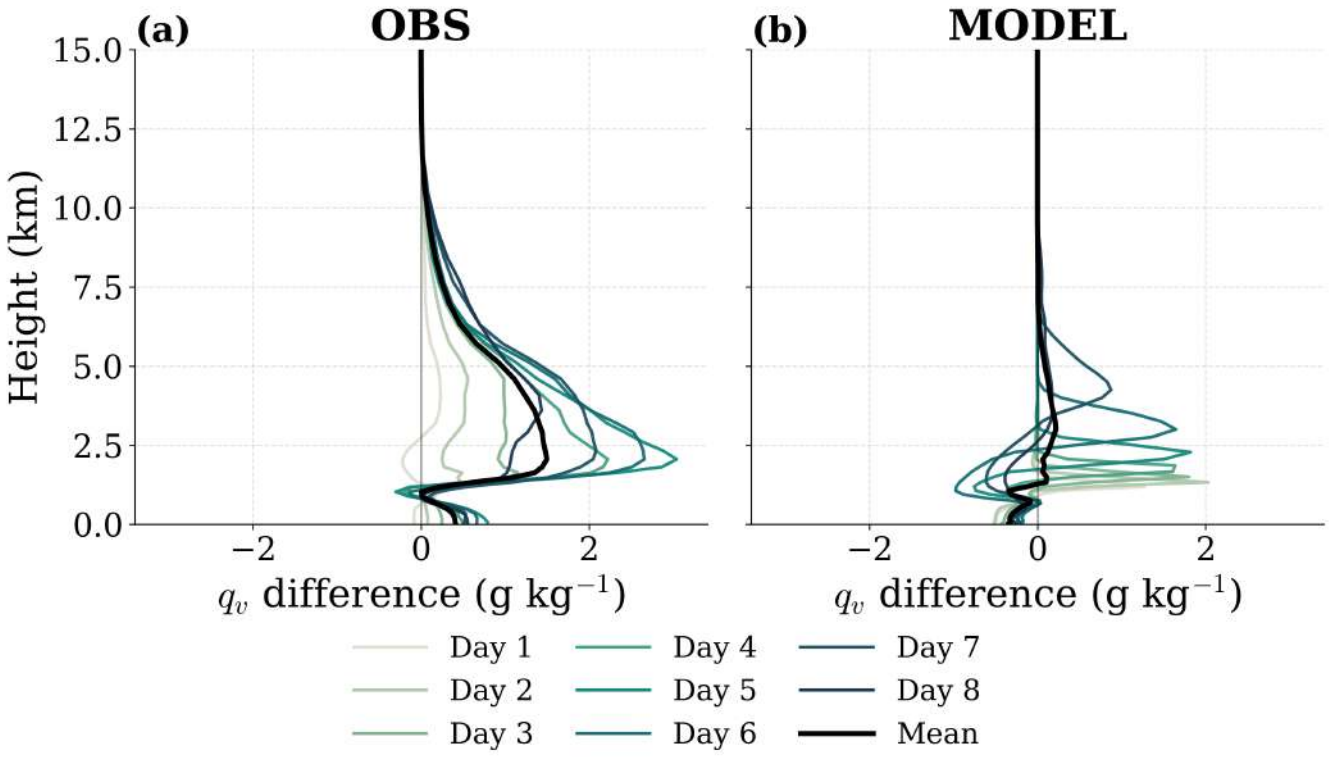

Figure S55. Daily (colors) and time-mean differences (black) in the vertical profile of specific humidity (q_v) between polluted and clean conditions from observations (panel a) and model simulations (panel b) at SEP2 (25.0°S, 75.0°W).

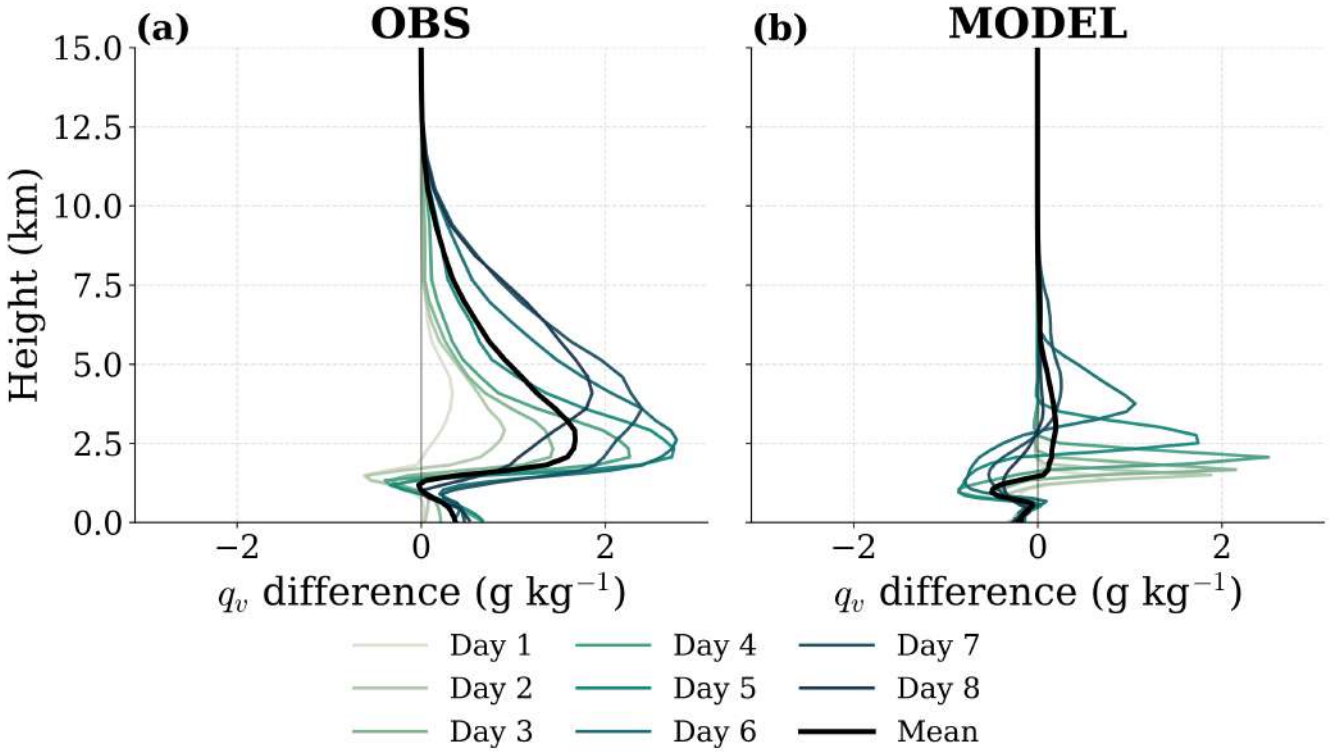

Figure S56. Daily (colors) and time-mean differences (black) in the vertical profile of specific humidity (q_v) between polluted and clean conditions from observations (panel a) and model simulations (panel b) at SEP3 (20.0°S, 80.0°W).

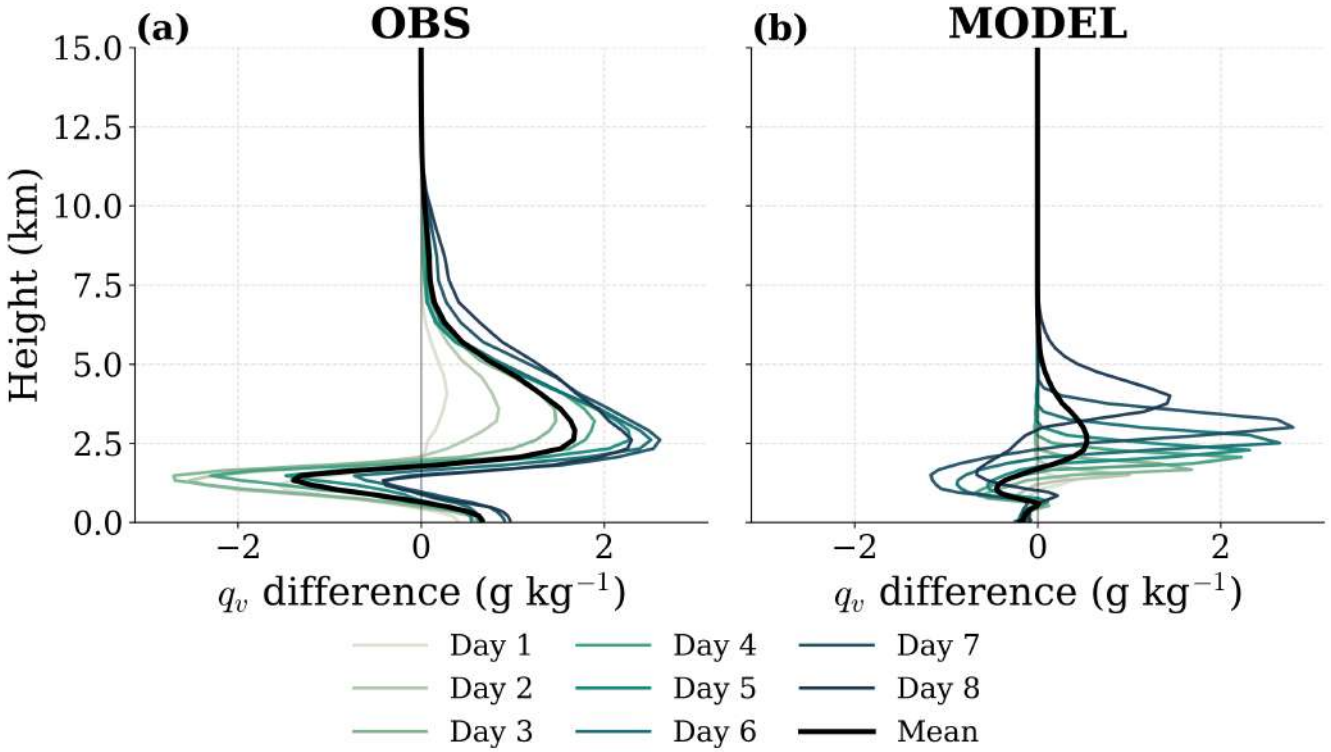

Figure S57. Daily (colors) and time-mean differences (black) in the vertical profile of specific humidity (q_v) between polluted and clean conditions from observations (panel a) and model simulations (panel b) at SEA1 (30.0°S, 10.0°E).

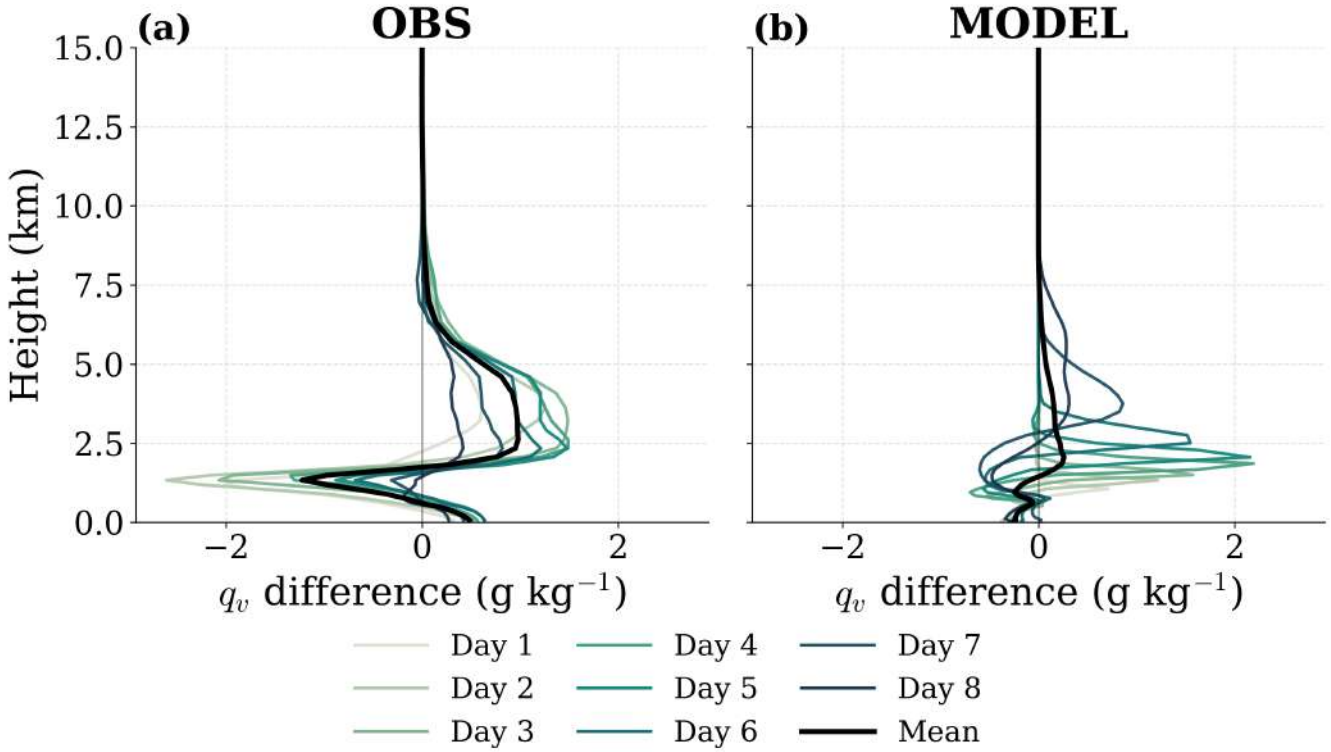

Figure S58. Daily (colors) and time-mean differences (black) in the vertical profile of specific humidity (q_v) between polluted and clean conditions from observations (panel a) and model simulations (panel b) at SEA2 (25.0°S, 10.0°E).

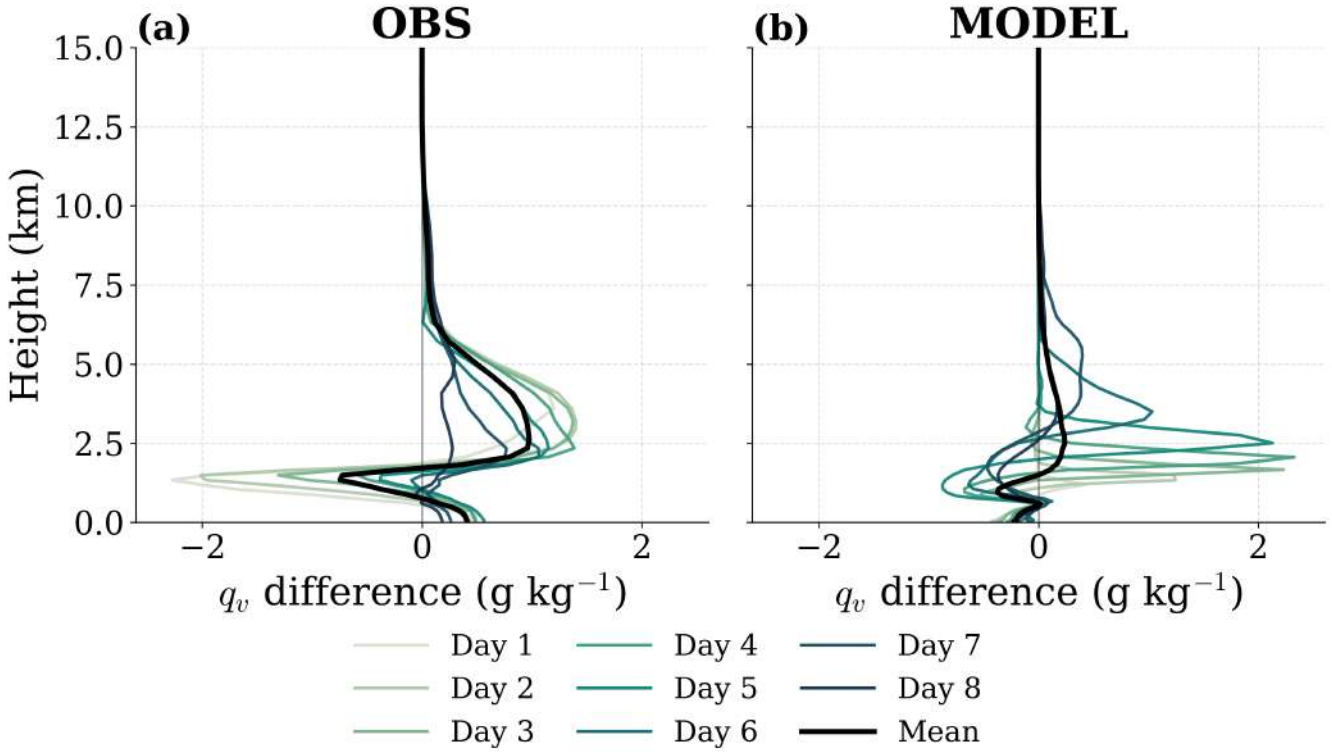

Figure S59. Daily (colors) and time-mean differences (black) in the vertical profile of specific humidity (q_v) between polluted and clean conditions from observations (panel a) and model simulations (panel b) at SEA3 (20.0°S, 5.0°E).

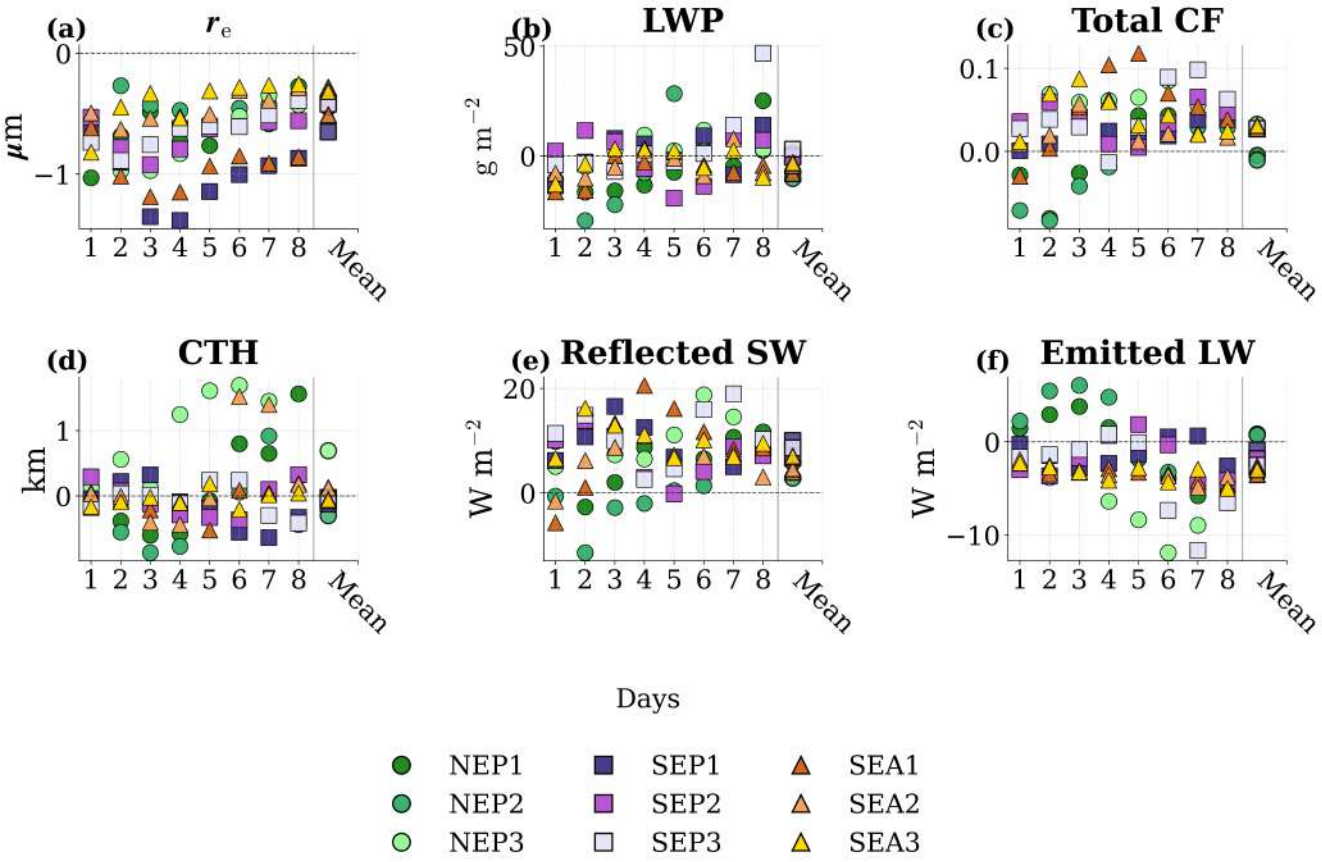

Figure S60. Daily mean differences between polluted and clean trajectory groups for all nine initiation locations (NEP1-NEP3, SEP1-SEP3, and SEA1-SEA3) based on observational data, divided according to (SO_4) at the 910hPa level. Panels show: (a) cloud droplet effective radius (r_e), (b) liquid water path (LWP), (c) total cloud fraction (CF), (d) cloud top height (CTH), (e) reflected shortwave radiation at top of atmosphere (Reflected SW; TOA), and (f) emitted longwave radiation at TOA (Emitted LW). Marker shapes and colors indicate the location, with dots representing NEP, squares representing SEP, and triangles representing SEA. The markers in the "Mean" column at the right of each panel represent the time-mean difference across all days.

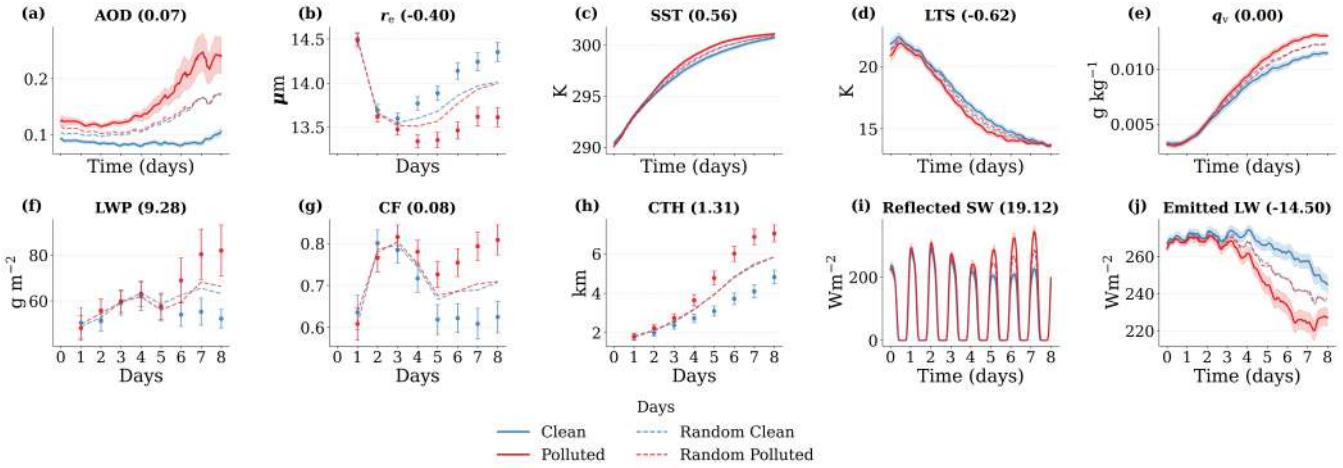

Figure S61. Evolution of aerosol, environmental, cloud, and radiative properties for the NEP1 initial location (34.0°N, 125.0°W), separated into clean (blue) and polluted (red) groups. Panels show (a) aerosol optical depth (AOD), (b) droplet effective radius (r_e), (c) sea surface temperature (SST), (d) lower-tropospheric stability (LTS), (e) specific humidity at 850 hPa (q_v), (f) liquid water path (LWP), (g) cloud fraction (CF), (h) cloud-top height (CTH), (i) reflected shortwave (SW) flux, and (j) emitted longwave (LW) flux. Dashed curves in each panel show the evolution of each variable for the seasonally bootstrapped (1000 times) reference groups (blue: randomized Clean; red: randomized Polluted). These randomized groups are generated by sampling trajectories from the full dataset while preserving the seasonal distribution and sample size of the original Clean and Polluted groups, but without conditioning on AOD. This provides a benchmark for variability expected from seasonality alone.

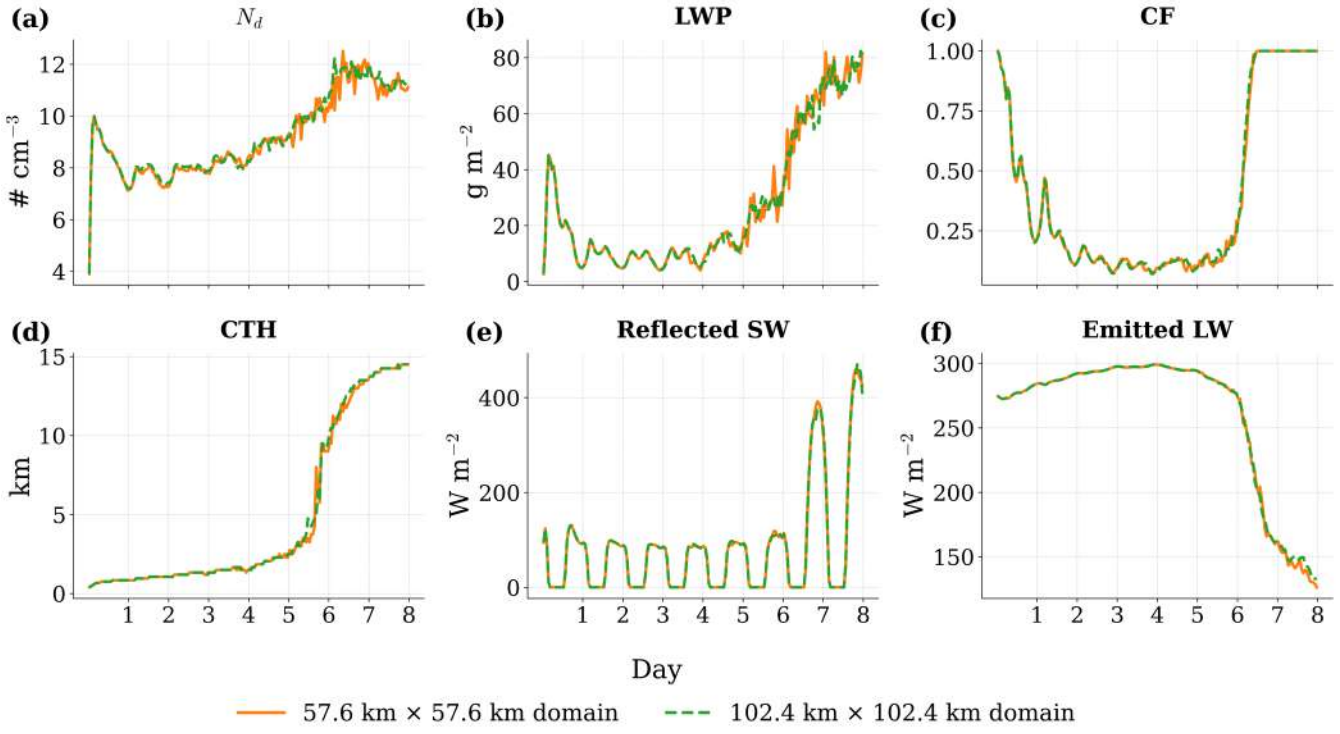

Figure S62. Sensitivity of simulated cloud and radiative properties to domain size for the NEP1 case. Time evolution of (a) droplet number concentration (N_d), (b) liquid water path (LWP), (c) cloud fraction (CF), (d) cloud-top height (CTH), (e) reflected shortwave (SW) flux, and (f) emitted longwave (LW) flux. Results are shown for simulations with domain sizes of $57.6km \times 57.6km$ (288×288 grid points; orange) and $102.4km \times 102.4km$ (512×512 grid points; green dashed).

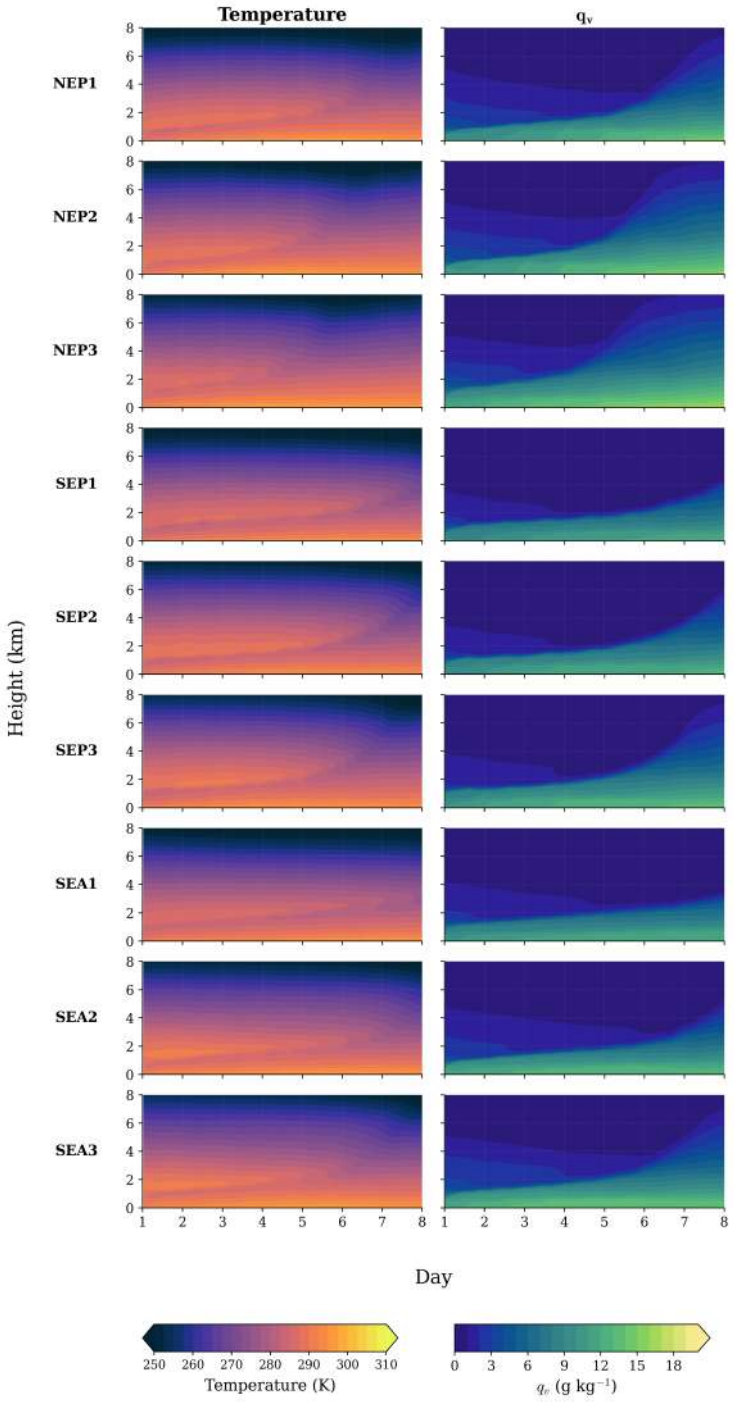

Figure S63. Hovmöller diagram of temperature (left column) and specific humidity (q_v; right column) along the different clean model simulations for all nine initiation locations (NEP1–NEP3, SEP1–SEP3, SEA1–SEA3). Color scales are shown under each column.

S2 Additional Tables

Table S1. Number of trajectories that individually satisfy each filtering criterion at each initial location. Each entry shows the number of trajectories passing the given filter when applied independently. The total number of trajectories per location is 1827. The filtering criteria are as follows: the latitude flow filter selects trajectories that move equatorward; the longitude flow filter retains those that advect westward under the trade-wind flow; the poleward constraint removes trajectories that deviate poleward of their starting latitude; the low land fraction filter excludes trajectories influenced by land; the low SST variability filter removes trajectories that go over the sea-surface temperature standard deviation of 4;

Filter	NEP1	NEP2	NEP3	SEP1	SEP2	SEP3	SEA1	SEA2	SEA3
Latitude flow	1243	1377	1125	1629	1750	1797	1426	1798	1818
Longitude flow	1136	1436	1424	1454	1515	1694	1398	1340	1619
Poleward constraint	1237	1426	1255	1558	1723	1783	1406	1780	1813
Low land fraction	1316	1604	1622	1307	1259	1700	1415	984	1166
Low SST variability	1160	1626	1615	1413	1475	1768	1513	1691	1791